Escola de Camins
Escola Tècnica Superior d'Enginyeria de Camins, Canals i Ports
UPC BARCELONATECH

TESI DE MÀSTER

Màster

Màster Universitari en Enginyeria de Camins, Canals i Ports

Títol

Experimental and Numerical study of capillary flow in cracked cementitious materials

Autor

Berta Gimeno Ferrer

Tutor

Jesús Miguel Bairán García

Intensificació

Enginyeria d'Estructures i Construcció

Data

Juliol, 2014

Acknowledgements

I would like to thank my mother and father for which this TFM is dedicated to this would not possible without their love and support.

Dr. Diane Gardner my external tutor has assisted me through learning and she has taught a lot.

Dr. Jesus Bairan my home tutor had transacted all my workpapers.

The technician staff: Carl, Ian and Harry have been amazing and enjoyed every minute in the lab and helping in experimental difficulties.

Finally I would like to thank my husband to support me in each minute.

SUMMARY

This dissertation is concerned with the experimental and numerical study of capillarity flow in cementitious materials. This work is based on the previous research done by a team from Cardiff University, and tackle with the investigation on the capillary flow of water for a artificial (planar) and natural crack configuration in discrete cracks in concrete.

Experimental simulations of capillary flow using three different concrete mixtures (C20, C30 and C50) it has been evaluated in order to quantify the effects of the compressive strength and the specimen age in the capillary rise response.

Alongside the experimental work, a numerical model based in the amended Lucas-Washburn equation proposed by Gardner et al. (2012) has been built, and the values for the correction parameters for pinning, friction dissipation and wall slip has been adjustable in order to fit the new experimental data from the artificial crack tests.

Some of the conclusions that have been made are that the results looking at the effect of the concrete strength show that it was not founded a clear relation between the capillary rise response and the concrete strength, and the specimen age of concrete affected the rate of rise, being faster in young specimens and producing a retardation in matures. These remarks have been use in order to estimate the correction parameters in the amended Lucas-Washburn equation.

Finally a new function for concrete based on the function for mortar published by Gardner et al. (2012) that relates an equivalent planar opening with a mean aperture of a natural crack have been generated from the natural crack results, updating their original values.

Contents

List of Figures

List of Tables

1 INTRODUCTION

1.1 Background

Concrete is the second most consumed substance in the world after water, and its usage is twice as much as wood, steel, plastic and aluminium combined. In 2012, this industry produced approximately 3.6 billion tonnes of cement per year mostly in Asia (Figure 1-1), making it the most abundant man-made product in the world (de Rooij et al. 2013).

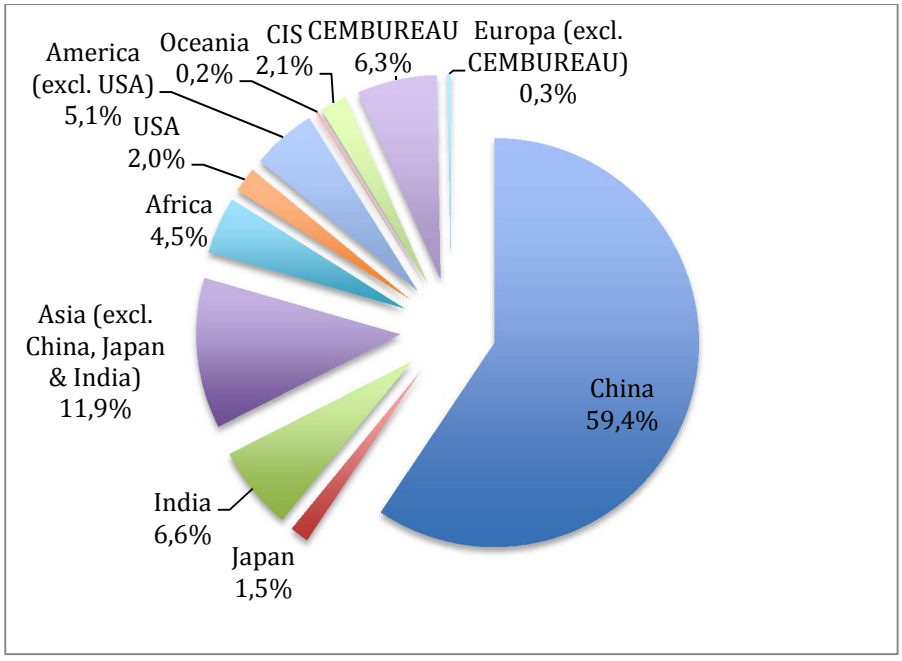

Figure 1-1. World cement Production in 2012 by region and main countries. Figure reproduced from IMF World Economic Outlook 2013, April 2013

In Europe, the cement and concrete industry is critical for the economy with a turnover of more than €100 billion a year and around 500.000 persons employed (Table 1-1). Furthermore, civil engineering infrastructures represent about 70% of the national property.

	Enterprises (thousand)	Turnover (€ million)	Value Added (€ million)	Person employed (thousand)
Cement and concrete	27,3	113168,0	35397,0	545,2
Cement, lime and plaster	1,3	26723,0	10586,0	81,6
Articles of concrete, plaster, cement	26,0	86445,0	24811,0	463,6

Table 1-1. Cement and concrete production statistics - NACE Rev. 1.1. Table reproduced from Eurostat (SBS), 2006

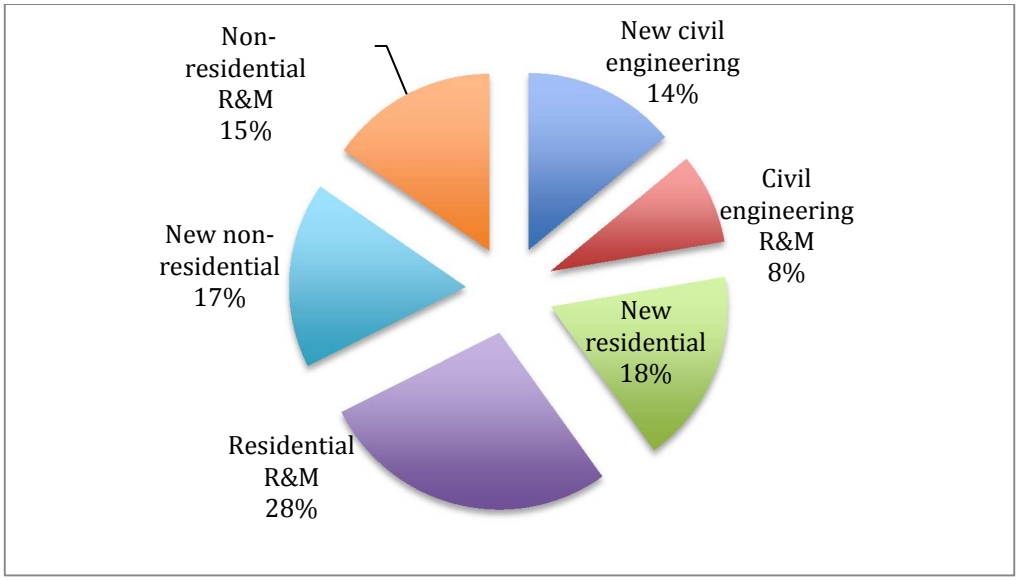

Figure 1-2. Construction in Europe – Breakdown in 2012. Figure reproduced from EUROCONSTRUCT, VTT, Buildecon

It is well known that tensile resistance of concrete is far slower than the compressive, and consequently reinforcement is required. Regardless, cracking is produced, and below to a limit crack width, accepted. Additionally, when the cracks are too wide, they can lead to a reinforcing steel corrosion, which affects seriously the durability of the structural concrete and ultimately can produce the collapse of the reinforced concrete.

In 2012, construction in Europe budged €1.291 billion, however renovation and maintenance (R&M) constituted more than a half (57%) of the total expenditure (Figure 1-2). In fact, according to Söderqvist (2003), the operation, maintenance, repair, rehabilitation, and renewal of the public civil infrastructure consumes about 35% of all energy and represents 30% of all environmental burdens and wastes. A cost of deterioration study released in 2002 by NACE for the U.S. Federal Highway Administration (FHWA) (NACE 2002), shared that the annual direct cost of corrosion in highway bridges is approximately $8,3 billion in the United States.

In concrete the corrosion of reinforcing steel may be caused indirectly by carbonation or chloride or well it can exist as a direct degradation of concrete produced by freeze/thaw attack (internal damage, scaling), acid action (dissolving action), or reactivity of aggregate (internal damage) (fib 2013).

All this phenomena affects the durability of structural concrete components in service, which is determined by the transport of aqueous and gaseous substances in the pore system of concrete and their interaction with the hydrated paste matrix, aggregate or steel reinforcement (fib 2013). Moreover, cracks produced by plastic shrinkage, creep, structural loading or early thermal effects may facilitate the ingress of the damaging substances leading to concrete deterioration. Thus, not only macro-cracks but also micro-cracks, caused for example in early ages by thermal effects or plastic shrinkage, produce concrete deterioration because facilitate the introduction in the concrete of the aggressive substances.

Historically, the way to tackle with the deterioration and loss of durability has been the maintenance and repairing, assuming material deterioration as inevitable. But these methods can be very expensive, especially if maintenance is not regularly performed as De Sitter's entitled "Law of Fives" (De Sitter 1984) explain: each time that the maintenance is postpone to a later phase of deterioration, the repairing cost multiplies by five.

Consequently, it is necessary improve the durability of concrete in order to decrease the cost of renovation and maintenance. Several techniques have been developed over many years. The most known include the use of waterproofing admixtures, glass fiber reinforced concrete or low porosity high strength concrete. However, another point of view based in the imitation of biological systems, and the way how the organisms are able to seal their wounds, has been developed recently: The self-healing materials (Lark 2013).

These materials, named "smart" materials, have the ability to self-repair the cracks and consequently enhance their service life (Joseph et al. 2010a). In the last decade, the interest for these materials has kept growing with the support of the organization of four international conferences on self-healing Materials, the establishment of several groups of research such as Self-healing concrete (TUDelft) or Materials for life (M4L) (Lark 2013) and a specific RILEM committee in Self-Healing Phenomena in Cement-Based Materials (de Rooij 2013).

The self healing materials can have specific advantages in comparison with the traditional cementitious materials in several fields where the enhanced durability plays an important role for example, in structures with a long service life (dams…), in infrastructures overexposed to adverse environment and climatic conditions (buildings near the coast line, chemical industries…), in structures located in places with a difficult access (high mountains spots, off-shore installations, underwater or underground locations…), in public works where the crack width is critical (water storage structures, strategically installations …) or in specific situations where the maintenance works can led to a high social cost (traffic jams derived from repairs works in the motorways…) (de Rooij et al. 2013).

On the basis of the origin of the components involved in the recovery process in the self-healing cementitious materials, they can be divided in two groups (de Rooij et al. 2013),

- autogenic healing (“own generic materials”), that is the natural ability of concrete to self-repair
- autonomic healing (“engineered additions”), that is when the concrete has been manufactured to have the ability to self-heal.

The autonomic healing uses components that naturally are not found in the material. Usually, the foreign material is an adhesive agent that are embedded inside the matrix of the concrete in a container that could be a tube or capsule, and when it breaks is activated and disperses the chemicals. Later, the healing agent flows under capillary action to the cracks (Figure 1-3). According to Joseph et al. (2010a), this technique has a big potential in the construction industry and he specified that the most commonly adhesive agent used have been: cyanoacrylates (superglues), epoxy resins, alkali-silica solutions and polyurethane.

Cyanoacrylates typically have a shelf life of one year. When encapsulated within concrete they would be expected to heal damage that occurs within the early life of a structure. However, the future development of flow networks may offer the potential to continually deliver superglues and resins to zones of

damage throughout the working life of a structure thereby removing the constraint of the healing agent's shelf life.

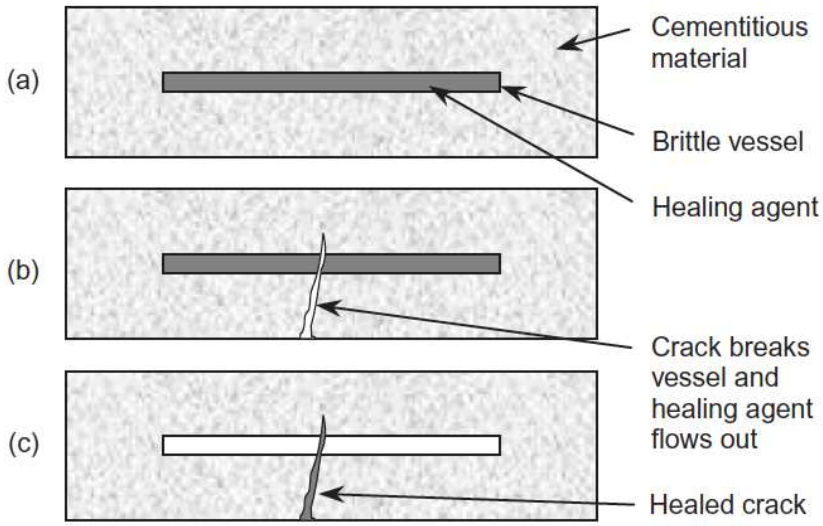

Figure 1-3. Autonomic healing concept in cementitious materials. Figure reproduced from Joseph et al. (2010b)

Numerous experimental studies have been performed on capillarity in porous media with the majority of researchers using sorptivity as a measure of capillarity. It is evident that few researchers have considered capillary flow in a single capillary (i.e. a discrete crack) and the studies which are available offer limited data due to the low number of crack apertures and configurations employed. Numerical simulations and predictions of capillary absorption in cementitious materials have been presented by a number of researchers, although again a far greater body of work has been published on capillary rise in porous media in general, rather than in concrete in particular (Gardner et al 2012).

However, in the last years a team from Cardiff University has been conducting several studies with the purpose of better understanding the capillary action of healing agents in discrete cracks. These studies have provided new experimental data on the capillary flow of water and some adhesives, mainly cyanoacrylates, in discrete cracks in cementitious materials and furthermore, they have amended a numerical model for capillary flow based in the Lucas-Washburn equation and propose a relationship in the capillary rise response between different cracks shapes.

1.2 Aims of the project

As mentioned above, it is crucial to study deeper the mechanism of the capillary flow of the healing agent in order to evaluate and predict the potential and the efficiency of the healing process, always thinking in the final objective of develop a new generation on cementitious materials.

The previous work have proved that the experimentally observed capillary flow in cementitious materials does not fit perfectly with the standard Lucas-Wasburn theory and therefore, it seems perfectly reasonable to have a better understanding of the capillary rise conducting further studies that take a closer look in the parameters that influence the flow.

The dissertation is mainly based on the experimental work carry out by the team at Cardiff University in the last years mentioned above. This work was extended doing new tests with the following characteristics:

The experiments were conducted with water in concrete with three different compressive strength (C20, C30, C50) and two different crack configurations were studied: Planar with different range of crack apertures and one year's old samples, and natural with crack apertures of 0,5, 1, 1,5 and 2 mm and seven day's old specimens.

The particular aims of this study were:

Firstly, evaluate the effect of curing and the influence of the different roughness of the concrete wall surface by using mature (365 day old) specimens (only one kind of mortar with a maximum of 28 days of curing have been studied so far).

Secondly, adjust the relationship proposed by Gardner et al (2012) that relates the natural crack aperture with an equivalent planar crack width by including examining flow in larger natural crack apertures in concrete. This function gives the planar aperture that have the same capillary rise behaviour as that of a known natural crack width for a mortar. In this study, three different strength concrete mixtures were studied in order to find an accurate function in wider openings and furthermore, prove if exists a dependency of the function with the concrete strength.

Finally, provide more experimental data to validate and improve the proposed

numerical model based in the Lucas-Washburn equation and its corrections factors in order to simulate the observed results.

The present investigation concentrates on flow in a discrete crack with no consideration being given to flow into or out of the porous media adjacent to the discrete opening

1.3 Relevance to beneficiaries

The relevance to the beneficiaries and the potential impact can be analyzed quantitatively in terms of direct savings and social savings. The former include the economical cost and the latter the negative externalities in the environment for example. In the recent decades, due to the present concerns about the environment issues is growing stronger the new approach of the sustainable engineering where the projects must be analyzed bearing in mind additional criteria beyond the traditional time-cost-quality triangle in the Life-cycle assessment (Fenner et al. 2006) (Figure 1-4).

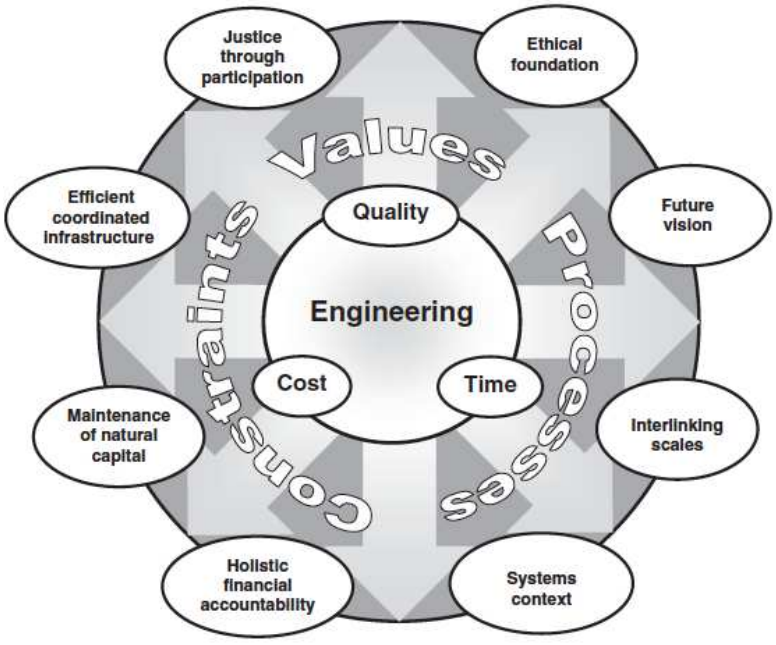

Figure 1-4. A sustainable framework for engineers. Figure reproduced from Fenner et al (2006)

It is clear that the initial investment for the construction industry using self-healing materials will be higher as an additional components and extra manufacture will be necessary. These extra charges are estimated at 20%

(Lark 2013). However, in the long-term the reduction in maintenance and the increase in their lifetime it will result in direct savings for the infrastructure whole-life cost that can arrive to 50% (Lark 2013).

On the other hand, several social savings can be derived from the use of these new materials. Works of repair and maintenance in roadways produces a significant proportion of the traffic jams, those indirectly have detrimental effects on productivity.

In a specific study carried out in Netherlands using a self-healing asphalt (de Rooij et al. 2013) it was shown that extend the lifespan of the asphalt by 50% can lead to an accumulative net savings up to 90 millions euros even when the cost of the new self-healing material is increased by 200% (Figure 1-5).

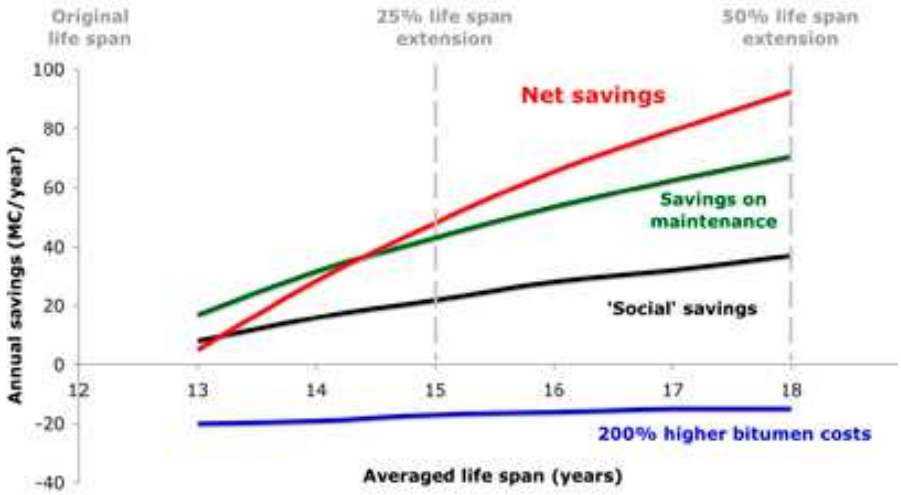

Figure 1-5. Annual net savings that can be achieved with self-healing asphalt considering direct and social savings, and higher initial cost. Figure reproduced from de Rooij et al. 2013

Another important point is regarding the carbon dioxide (CO2) emissions. The cement industry is one of the highest producers of carbon dioxide. The manufacture of 1 t of Portland cement implies the emission of 1 t of CO_2 gas. Consequently, only this industry is responsible of the approximately 6% of the anthropogenic CO_2 emissions in the world (de Rooij et al. 2013), and these figures are still growing as the global production of cement is rising boosted mainly for the Asian countries. An increment of the service life will decrease the necessity of new structures and hence minimize the carbon footprint of the cementitious materials.

Therefore not only the private sector in the construction industry can find in the self-healing materials a profitable niche, but also structures managers and maintenance authorities, structures contractors with construction and maintenance contracts, governments and the society can be a beneficiary.

Capillary flow plays a key role in order to evaluate the efficiency of a healing agent and hence reach a deep knowledge of this mechanism is basic to analyze the financial risk of self-healing process. Furthermore, the current investment for study the capillary flow in cracked cementitious materials could be useful indirectly in other fields such as soils contamination or long-term nuclear waste storage studies.

This dissertation will present in the following chapters a well-detailed description of experimental and numerical work conducted including the discussion of the results obtained.

2 LITERATURE REVIEW

2.1 Self-healing cementitious materials

Dry (1994) use the pioneering term of autonomic healing in cementitious materials, but this philosophy has been more developed in the last decade in a group of new polymers created by White (2001). However, there are some researches that have conducted further investigation with the encapsulation techniques in cementitious materials.

Li (1998) studied the healing agent cyanoacrylate in capillary tubes, Mihashi et al. (2000) experimented with microcapsules and continuous glass pipes and Joseph (2010b) with continuous supply networks.

On the other hand, to increase their rapid development and future profitability, the healing agents are generally low cost and widely available. The most commonly used have been (Joseph et al. 2010a): cyanoacrylates (superglues), epoxy resins, alkali-silica solutions and polyurethane.

In order to guarantee the success of the healing process, the healing agent must have low viscosity and furthermore it has to be able to create a strong bond between the fissure walls Joseph et al. (2010a). Nevertheless, it is also important consider the parameters related to the crack width, as this parameter highly influenced the forces involved in an autonomic self-healing system.

Joseph et al. (2010b) conducted a work in order to model the mechanism in an autonomic self-healing system. In the figure 2-1 are drawn the main forces that take place when the encapsulated self-healing agent is released and has to flow to the crack.

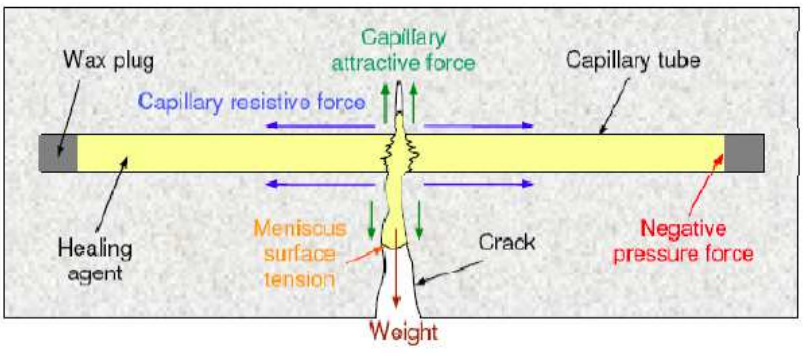

Figure 2-1. Schematic of the principal forces acting on an autonomic self-healing system. Figure reproduced from (de Rooij et al. 2013).

In the ascending direction, the main force acting is the capillary action, and in descending the gravity.

2.2 Mechanisms of transport in concrete

The movement of the fluids through concrete is highly related to the structure of the hydrated cement paste and takes place by three transport mechanisms (Neville 2011):

- Permeation refers to flow through a porous medium under a pressure differential (hydrostatic head)
- Diffusion is the process in which a fluid moves under an ion concentration gradient.
- Absorption is the fluid movement produced by capillary suction due to the surface tension acting in capillary pores.

The hydrostatic head is important only in structures that are permanently in contact with water like water storage structures. In the rest, meteorological phenomena such as rain or wind facilitate access to the concrete surface. As the diffusion takes place very slowly, capillary suction, mainly in unsaturated concrete, becomes the most relevant transport mechanism (Martys and Ferraris 1997).

2.3 Capillarity. Definitions

2.3.1 Physical phenomena. Wettability

Capillarity or capillary action is the ability of a liquid to rise in narrow spaces. It occurs because of the intermolecular interactions between the liquid and solid surrounding surfaces.

Cohesion is the name that represents the attractive forces that exists in a liquid between its equal molecules (the liquid sticks to itself). These forces are the responsible for the phenomenon known as surface tension, denoted by γ(N/m).

Thanks to the surface tension a liquid can resist an external force and the formation of water droplets is possible, because on the surface of the liquid the molecules are not surrounded by other molecules like them on all sides (unlike the molecules in the bulk of the liquid), and consequently, the net force is not zero and is drawn inwards creating an internal pressure.

On the other hand, adhesion is the name that represents the attractive forces that exists in a liquid between different molecules, such as the ones from a liquid and a solid surface (the liquid sticks to other materials).

The balance of the adhesive and cohesive forces determines the liquid's ability to wet a solid surface (wettability).

When the adhesive force between the solid surface and the liquid is greater than the surface tension produced by cohesion inside the liquid, the meniscus is formed on the edge of the surface. If the surface walls are sufficiently near each other, the combination of these forces acts to lift the liquid inside the solid surface producing the capillarity (Lerner and Lerner 2004).

2.3.2 Contact angle

The wettability is related to the liquid-solid contact angle (θ), that is the angle between the solid-liquid interface and the liquid-gas interface, as seen in the figure 2-2.

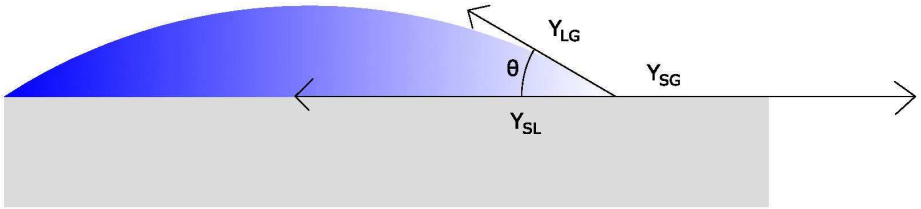

Figure 2-2. Schematic of the interfaces and the contact angle (θ) of a fluid on a solid surface.

The Young's equation gives the relation $\gamma_{SG} - \gamma_{SL} = \gamma_{LG} \cdot \cos\theta_c$ (Chow 1998), where the surface tension (γ) are expressed in terms of interfacial energy per unit area. If the contact angle (θ) is < 90º, the wettability is very high and the liquid tends to spread across the surface, as it happens for example with water and ethanol in a glass tube, which have a θ = 0º (perfect wettability).

2.3.3 Capillarity equation

At the beginning of the 20th century Washburn (1921) conducted a pioneering work on the kinetics of capillary penetration of liquids into circular cylindrical capillaries and porous bodies, and employing a force balance between a driving capillary force and a retarding viscous force formulated the Lucas-Washburn equation (2-1):

$$h = k \cdot t^{1/2} \qquad (2\text{-}1)$$

where “h” is the capillary rise height (m), “t” the capillary rise time (s), and “k” the capillary coefficient (m·s$^{-1/2}$), that can be expressed as $= \sqrt{\frac{\gamma r cos\theta}{2\mu}}$, with: γ = surface tension (N/m); r = radius of the capillary(m); θ = liquid/solid contact angle(°); and μ = dynamic viscosity (Ns/m^2).

However, several articles such as Liou et al. (2009) describe the complete Lucas-Washburn equation with four terms (surface tension, gravity, viscous and inertial) starting from the Navier–Stokes equations. These terms represent the different acting forces, and in function of the time stage, all the terms can be dominant or neglected. Fries and Dreyer (2008) discusses the existent capillary rise analytic solutions in the literature for any of these time stages, that goes from purely inertial in the very first moments (Quere 1997), visco-inertial (Bosanquet 1923), purely viscous in the intermediate stage (Washburn 1921) and viscous and gravitational time at the later stage (Fries and Dreyer 2008) (Figure 2-3).

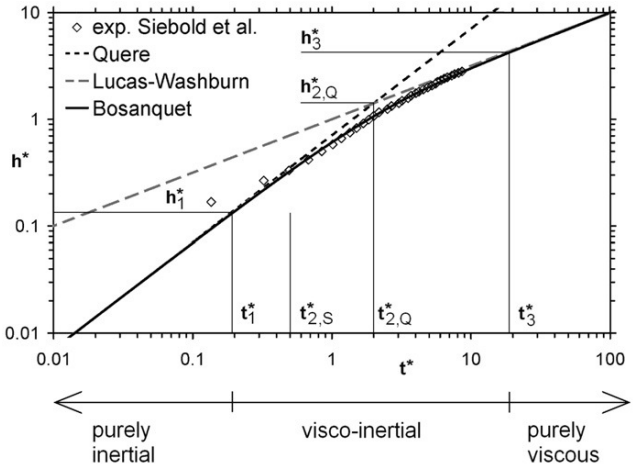

Figure 2-3. “Schematic dimensionless diagram showing an overview of the initial time stages of capillary rise”. Figure reproduced from (Fries and Dreyer 2008).

2.4 Measurement of absorption

In order to measure the absorption, several test methods exist, such as the Initial surface absorption test (ISAT), the Figg water absorption test and the Covercrete absorption test (CAT). However, there are some reported difficulties associated with these absorption tests (Neville 2011), therefore the capillary absorption is usually measured using an alternative type of test, the sorptivity

test which is now widespread used in construction materials (Hanzic and Ilic 2003).

2.4.1 Sorptivity

The Sorptivity test determines the rate of penetration of the capillary rise (sorptivity) by a concrete prism (Neville 2011). It is known (Hall 1989) that a relationship of the form exists (2-2):

$$i = S \cdot t^{1/2} \qquad (2\text{-}2)$$

where "S" = sorptivity (slope) (mm/min$^{0.5}$), "t" time since the beginning of the testing when the mass is measured (min), and "i" the volume of liquid absorbed (mm), that can be expressed as i = Δw / (A·ρ), with:

Δw = increase in weight (g); A = cross-sectional area in contact with the fluid(mm^2);and ρ = density of water (g/mm^3).

Several researches such as Hall (1989), Martys and Ferraris (1997) and Hanzic and Ilic (2003) have studied the sorptivity of cementitious materials and its dependence on different parameters such as fluid properties, pore structure (porosity, density, mixture composition, degree of compaction and curing), temperature and initial moisture content of the concrete at the time of testing (degree of saturation).

Hall (1989) compiled sorptivity data from several cementitious material and showed in the figure 5 how the sorptivity was influenced by the mixture and the compaction. In the mortars mixes (figure 2-4a) were observed that the sorptivity rose with lower density, and also a correlation with the water/cement ratio existed. However, in the concrete mixtures (figure 2-4b) the relation between density and sorptivity was less clear, and the dependence with the W/C was null, revealing that were many others parameters that influence as for example the method of sample preparation.

On the other hand, sorptivity decreases with the increment of the initial water content and with longer curing periods due to the reduction of the pore size (Martys and Ferraris 1997). Furthermore, the sorptivity is proportional to the quantity $(\gamma/\mu)^{1/2}$ and therefore the sorptivity increases with higher temperatures and it varies with different fluids (Hall 1989).

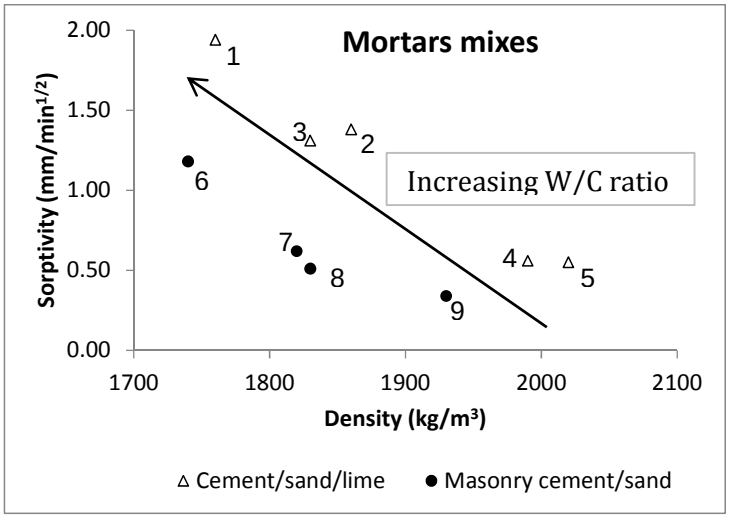

a)

Cement/Sand/Lime	W/C ratio	Sample
1:3:10	3,20	1
1:2:8	2,20	2
1:1:5	1,55	3
1:0,5:4	0,93	4
1:0,25:3	0,85	5
Mas, cement/Sand	W/C ratio	Sample
1:7	1,15	6
1:6	1,10	7
1:5	0,95	8
1:3	0,63	9

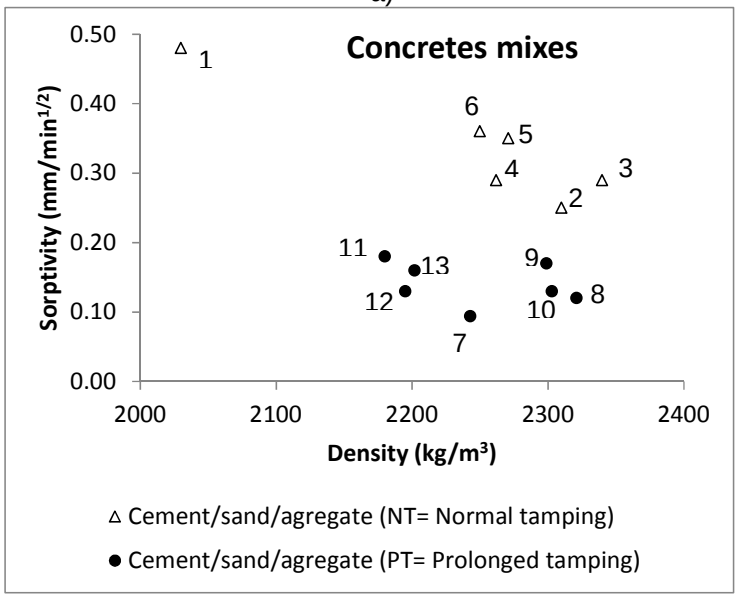

b)

Cement/Sand/ Aggregate	W/C ratio	Sample	
		NT	PT
1:2:4	0,4	1	7
1:2:4	0,5	2	8
1:2:4	0,6	3	9
1:2:4	0,7	4	10
1:2:4	0,8	5	11
1:2:4	0,9	6	12
1:2:4	1,0		13

NT = Normal tamping
PT = Prolonged tamping

Figure 2-4. Sorptivity data in mortars and concretes. Figure reproduced from Hall (1989)

2.4.2 Relationship between sorptivity and capillary rise in concrete

Hanzic and Ilic (2003) studied the relationship in concrete between sorptivity "S" measured using a Sorptivity test, and capillarity rise "h" measured by means of the Neutron radiography (NR) technique. They analysed water and fuel oil in mixtures of concretes with several additives obtaining different results and concluded that S and h are not always coincident, for this reason large sorptivity does not necessarily mean high capillary rise, and consequently a direct measurement of the capillary rise "h" was therefore deemed necessary.

2.5 Influence of crack configuration

Collins and Sanjayan (2008) argued that the tortuosity and the surface roughness can be a source of errors in the measurement of the capillary rise in unsaturated concrete.

2.5.1 Tortuosity

Liou et al. (2009) proposed an analytical numerical model in order to study the effect of a non-uniform geometry on the capillary rise in tubes.

They introduced the non-uniformity effect in the terms of the complete Lucas-Washburn equation where the velocity is involved, that is in the viscous and the inertia terms. In regard to the viscous term, they take into account the effect associated with the two viscous terms on the cross-sectional plane and the one associated with the axial viscous normal stress. The consideration of this last effect, together with the inertia term, are the main difference between the numerical equation proposed by Liou et al. (2009), and the model developed by Young (2004) for non-uniform capillaries.

The analytical model including the full viscous terms and the inertia term was validated using other studies of capillary-driven flows in different geometries that have already been analyzed by other researches. The first two cross sections were uniform and consisted in rectangular microchannels, studied analytically by Ichikawa et al. (2004) and experimentally by Jong et al. (2006) and in a circular cylindrical capillary, studied by Erickson et al. (2002) using finite-element-based numerical simulations. From the latter authors it was extracted the third test problem, a nonuniform geometry consisting in circular converging–diverging and diverging–converging capillaries, and in this particular case, the model was compared also with the results obtained using the Young (2004) equation. In all the situations, the Liou et al. (2009) numerical model agreed with the test problem.

Later, they examined three new non-uniform cross sections: the parabolic, the sinusoidal and the divergent sinusoidal capillary, and investigated the effect of the viscous and the inertial terms on the capillary flow.

However, it is not habitual to have the complete information of the fracture shape, so Gardner et al. (2012) proposed the equation (2-3) based on

correction parameters to find for a natural crack of known average opening, its equivalent artificial planar configuration opening.

$$C_{W_p} = k(\zeta) C_{W_n} \quad (2\text{-}3)$$

With:

$$k(\zeta) = \zeta k_0 + (1 - \zeta) k_m \quad (2\text{-}4)$$

$$\text{and} \quad \zeta = \left(\frac{C_{W_n}}{C_{W_e}}\right)^n \quad (2\text{-}5)$$

Where C_{W_e}= Threshold value of the crack aperture above which the capillary rise response for the planar and the natural crack is the same; k_0= "Gradient of the initial slope of the graph"; k_m = "Gradient of the graph as it becomes asymptotic to the crack convergence value" (Gardner et al. 2012).

The figure 10 shows the relationship between capillary rise in natural cracks and in an equivalent planar crack expressed by the equation 2-3.

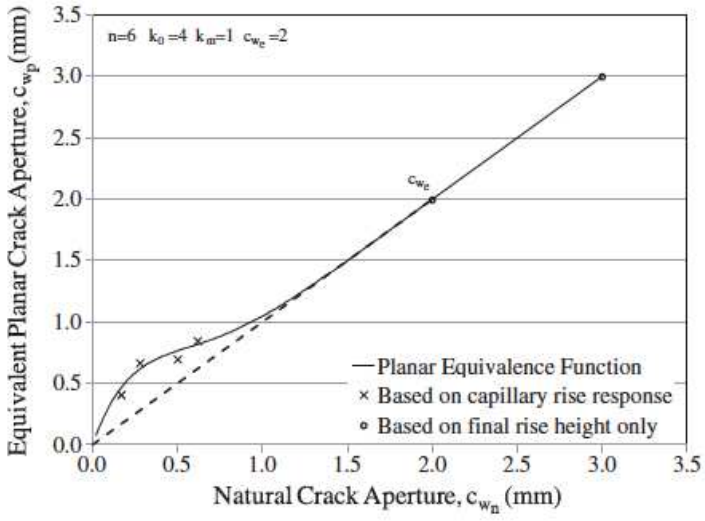

Figure 2-5. Function that relate an equivalent planar opening with a mean aperture of a natural crack. Figure reproduced from Gardner et al. (2012)

The authors assume with this function that after the C_{we} natural crack aperture, the influence of the roughness in the natural crack can be neglected, and consequently the final capillary rise height is the same than in the planar configuration. However, they specified that the roughness could be dependent of the maximum particle size in the concrete mixture and consequently further investigation is required with different crack openings and concrete mixtures.

2.5.2 Roughness

Schäffer and Wong (1998) experimented with several capillary columns with rough and smooth interior walls and observed that the solid wall roughness was the principal cause of pinning-depinning, a stick-slip movement phenomena that affects the dynamics of the capillary flow in a glass column.

This effect is function of the mortar age, because the curing changes the microstructure of the wall surface (the mortar it becomes drier and denser) and this produce a different roughness in the interface solid-liquid (Schäffer and Wong 2000).

The effect of the mortar age in the capillary flow of water was evaluated by Gardner et al. (2012) testing specimens after 7 days of curing against others with 28 days. The results showed that at the end of the experiments, the water reached a very similar capillary rise equilibrium height in both cases, although the rate at which this was achieved in the mature specimen was slower.

2.6 Influence of flow agent in capillary rise

Zhmud et al. (2000) studied numerically and experimentally the dynamics of capillary rise of two ethoxylated trisiloxane surfactant solutions in hydrophobic glass capillaries with radii of 0,1, 0,15, 0,25, and 0,5 mm. They specified that in this case the Lucas–Washburn equation might not work at all because the physics implicated in the surfactant transport are different.

Gardner et al. (2014) conducted an investigation focussed on the response of the flow agent cyanoacrylate. Analysing 28-day-cured specimens against 7-day-old, they found that the rate of capillary rise of the cyanoacrylate was slower in the younger mortar revealing a different behaviour from their study with water (Gardner et al. 2014) according to the flow agent in the interaction with the specimen characteristics. Previously, Gardner et al. (2011) had reported a higher equilibrium height in the older specimens, but this affirmation is not in agreement with the results showed by the same authors in 2014.

In addition, Gardner et al. (2011) reported that cyanoacrylate agent presented a smaller equilibrium height and slower capillary rate compared with water, not only because its flowing properties as contact angle or surface tension are different, but also due to the superglue curing modifies its viscosity during the

time course of the experiment. This effect was observed in cracks apertures up to 0,714 mm, and it was reported to be more noticeable in the narrower crack widths. This observation was reproduced again in Gardner et al. (2013) in the crack apertures of 0,05 and 0,1 mm.

2.7 Contact angle and capillary rise

The contact angle is usually measured using the sessile drop technique (Stalder et al. 2006). However, Hanzic et al. (2010) stated that several microscopic parameters exist which can produce disagreement with the observed value.

Siebold et al. (2000) proved with a series of experiments in glass capillaries that when a liquid moves rapidly over a surface, the contact angle changes its static value (θ_s) and becomes a dynamic contact angle whose value is a function of the liquid velocity contact line ($\theta(t)$). Fries and Dreyer (2008) noted that at the first stage of the capillary rise, when the flow rate is the highest, this can be a remarkable fact. Nevertheless, Fries and Dreyer (2008) specify that this initial period is very short, and in the later stages the dynamic contact angle can be neglected. However, Martic et al. (2003) emphasize that omitting the dynamic contact angle can lead to major errors in the capillary rise calculation so they proposed a modification to the Lucas-Washburn equation to take into account the velocity-dependent dynamic contact angle.

Previously, Hamraoui et al. (2000) had discussed the dynamic contact angle in terms of a microscopic friction coefficient following the model proposed by Blake (1993) who formulated a molecular-kinetic theory of liquids in order to explain the effect of the hydrodynamic forces on the dynamic contact angle. This approach focuses on the adsorption and desorption of the liquid molecules moving over a solid surface, and establish a microscopic friction that depends linearly with the velocity similarly to the macroscopic friction.

Later, the same authors Hamraoui and Nylander (2002) continued their study and expressed the discrepancies that they obtained between the analytic Lucas-Washburn equation and the experimental data with a retardation factor βm, related with the θ_t by the equation (2-6), and adopted the theory that the major contribution to the correction factor βm was the existence of an intrinsic

friction dissipation between the fluid and the solid at the region close to the moving three-phase contact line.

$$\gamma \cos[\theta(t)] = \gamma \cos(\theta_0) - \beta_m \frac{\partial h(t)}{\partial t} \quad (2\text{-}6)$$

$$\beta_m = \frac{\kappa_B T_v}{2\pi\lambda^3 \kappa_0^s \hbar} \eta \quad (2\text{-}7)$$

According to Blake (1993), all the parameters in β_m (equation 2-7) are microscopic, being "κ_B" the Boltzmann's constant, "T" the temperature, "v" the molecular volume of the fluid, "$2\pi\hbar$" the Planck's constant, " κ_0^s " the rate constant of the surface wetting adsorption process and finally λ the average distance between adsorption sites on the solid surfaces (Figure 2-6).

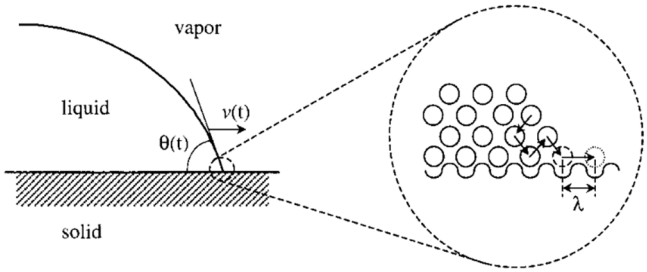

Figure 2-6. Schematic of microscopic parameters of the molecular-kinetic theory of wetting near the solid-liquid interface. Figure reproduced from Ruijter (1999)

This molecular length λ is difficult to measure and therefore Gardner et al. (2012) used the correction parameter βm as a material constant that has to be experimentally determined. Furthermore, Hamraoui and Nylander (2002) proved that at a macroscopic scale the parameter βm is intrinsic of the fluid/solid interaction and independent of the solid geometry (for example the capillary radius) and consequently for a whatever possible combination of a solid with a liquid, the β_m remains constant.

2.8 Modelling discrete cracks in cementitious materials

Roels et al. (2003) noticed that the presence of cracks in building materials should create preferential channels of flow that are frequently inadequately simulated by numerical models since they don't distinguish between the large differences in the fracture and the porosity of the media. To improve them, they presented a numerical stable prediction model using a moving front technique to solve through a combination of a quasi-static pressure equation and a

Darcian flux equation the waterfront movement in a discrete crack surrounded by a porous matrix media.

Roels et al. (2003) represented the discrete crack as a flow channel composed by pairs of parallel planar plates similar to several researches (Murphy and Thomson 1993, Wang and Narasimhan 1985) have done in order to model the flow in a single crack in geologic studies. In these models are always used a relationship between the Darcy's law and the cubic law that lead to an equivalent permeability term $k = b^2/12$, where b is the crack width instead of the capillary radius r (Zimmerman et al. 1992).

In order to validate the numerical model, Roels et al. (2003) performed laboratory experiments with two different fractured ceramic brick samples (artificial and natural fracture) using X-ray radiography to obtain greyscale images of the water rise at regular timesteps, which displayed good agreement with the prediction model.

Roels et al. (2003) used their numerical model to investigate the influence of the crack aperture and the material flow parameters in the water uptake in the fractured porous matrix. They noticed that the water absorption coefficient of the surrounding material matrix clearly influenced the rate of the water uptake in the crack itself, resulting in a retardation or even stagnation of the moisture waterfront when the fracture aperture is very small (microcracks) and, at the same time, the matrix absorption coefficient is very high.

The simulations conducted by Roels et al. (2003) with common concrete showed that in a crack aperture of approximately 0.1 mm or bigger, the waterfront in the fracture quickly (on the order of few seconds) reaches the topside of the specimen, without being influenced by absorption in the surrounding matrix.

The same team of researches went further into a posterior study (Carmeliet et al. 2004) and affirmed that the absorption only influences when the crack aperture is 0,02 mm or less. However, the investigation conducted did not analyse crack widths between 0,02 and 0,1 mm so it is considered a little unreliable without further experimental proof.

Gardner et al. (2012) studied the effect of the crack aperture (from 0.094 to 1.170), the age of the specimen (7 days of curing against 28 days) and the effect of the mortar saturation in the capillary flow rise height in different types of discrete cracks using water as a flow agent, and capturing its movement with a digital high speed MOTIONeer camera (Figure 2-7). In addition, Gardner et al. (2012) developed a numerical model based in the Lucas–Washburn equation in order to simulate the meniscus advance observed in the experimental test performed, although they proposed several corrections to the equation to take into account the stick–slip behaviour at the moving front, the frictional dissipation at the meniscus front and the wall slip.

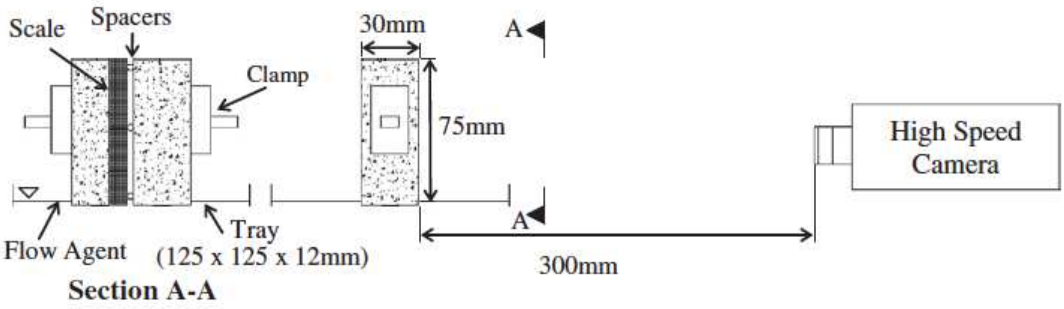

Figure 2-7. Configuration of the experiment. Figure reproduced from Gardner et al. (2012)

Delker et al (1996) conducted capillary flow experiments in columns filled with packed spherical glass beads and reported that the Washburn equation for capillary tubes reproduces correctly the behaviour in the short term. However, for large times, they observed that the water through the porous medium was following an algebraic and anomalous response far different from the Washburn's model.

Later, several number of researches as Lago and Araujo (2001), Lockington and Parlange (2004) and Shikhmurzaev and Sprittles (2012) emphasized the failure of the Washburn equation to describe the long term behaviour and provide an improvement over the formulation to try to explain the observed discrepancy. However, Gardner et al (2012) discussed that the experiments related with the capillary rise in a crack are always in the short time.

Finally, several studies have been recently conducted in self-healing porous asphalt pavements in order to prevent its deterioration. One method consist of the healing agent enclosed in the microcapsules embedded in the asphalt is

released when the fracture becomes big enough to contain the capsule. Later, the agent flows by diffusion into the crack (de Rooij et al. 2013). In other system, the bitumen itself is the healing agent and when reaches a threshold temperature, flows driven by capillary suction. García (2012) modelled this flow using an amended Lucas-Washburn equation and conduct several experiments where observed that the capillary rise begins in the aperture contact point.

2.9 Theoretical background. Numerical study

At the beginning of the 20th century Washburn (1921) conducted a pioneering work on the kinetics of capillary penetration of liquids into circular cylindrical capillaries and porous bodies.

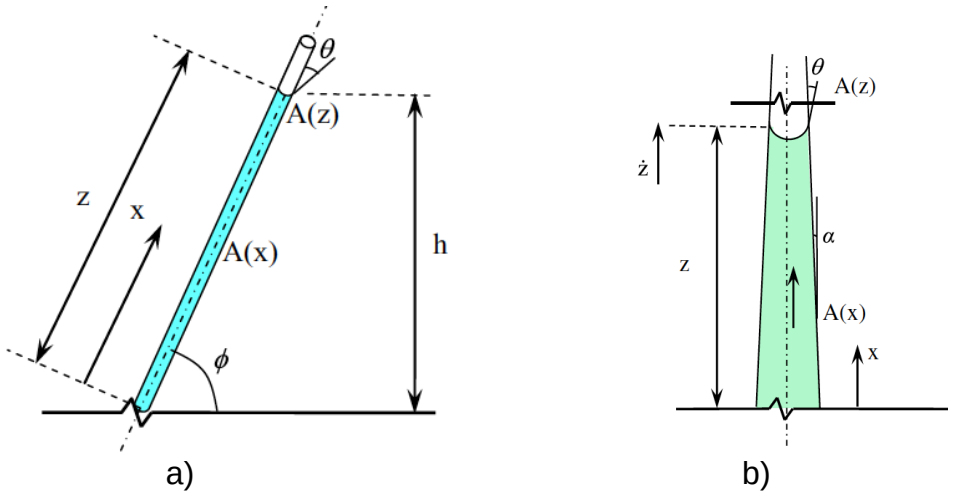

Figure 2-8. Illustration of the parameters used to model water flow in a a) uniform capillary b) non uniform capillary. Figures reproduced from Gardner et al. (2012) and (2014)

In the studies conducted by Gardner et al (2012 and 2014) the Lucas–Washburn equation has been the basis for describing the capillary absorption phenomena, and employs a force balance between a driving capillary force and a retarding viscous force. Later, to complete the momentum balance, there were included the gravitational and inertial terms.

$$2\pi r\gamma\cos\theta - \pi r^2\rho g z\sin\varphi - 8\pi\mu z\dot{z} - \pi\rho r^2\frac{\delta}{\delta t}(z\dot{z}) = 0 \quad (5) \qquad (2\text{-}8)$$

Where:

z = capillary rise height (m);

γ = surface tension (N/m);

θ = liquid/solid contact angle (°);

φ = capillary inclination angle (°);

ρ = is the density of liquid (kg/m3);

g = gravitational acceleration (m/s2);

r = radius of the capillary (m);

μ = dynamic viscosity (Ns/m2);

t = capillary rise time (s);

In equation (2-8) the individual terms refer to (left to right):

- The capillary pressure;
- The gravity term (hydrostatic pressure);
- The viscous pressure loss (Hagen–Poiseuille);
- The inertia term.

The inertial term can be omitted as has been justified previously by Gardner et al. (2012). Setting the inertia term to zero and dividing by π and r^2 gives the following equation of capillary flow.

$$p_c - \rho g z \sin\varphi - \frac{\mu}{k}(z\dot{z}) = 0 \qquad (2\text{-}9)$$

Where:

Effective permeability term $k = \frac{r^2}{8}$

Young-Laplace equation for capillary pressure:

$$p_c = \frac{2\gamma\cos\theta}{r} \qquad (2\text{-}10)$$

At static equilibrium ($z\ (t \to \infty)$):

$$h_{eq} = \frac{p_c}{\rho g \sin\varphi} \qquad (2\text{-}11)$$

Where:

h_{eq}= equilibrium capillary liquid rise height from balance of hydrostatic and capillary force

The corrections factors applied are:

$$p_{ceff} = p_{c0}(1 - \beta_s) \quad (2\text{-}12)$$

$$\beta_s = 1 - \frac{h_s}{h_{eq}} \quad (2\text{-}13)$$

Where:

β_s= correction factor for stick-slip behavior of the meniscus (unitless)

h_s = the rise height allowing for pinning (modified capillary rise height);

$p_{c0} = \frac{2\gamma\cos(\theta_0 - \alpha)}{r}$ where θ_0 is the static contact angle (°) and α is the inclination of the capillary wall (°). (2-14)

$$\gamma\cos\big(\theta(t)\big) = \gamma\cos(\theta_0) - \beta_m\dot{z} \quad (2\text{-}15)$$

Where:

β_m= correction factor for frictional dissipation at the moving front (units Ns/m^2)

$$\dot{z} = \left(\frac{r\beta_w}{2} + \frac{r^2}{8\mu}\right)\left(\frac{p_c}{z}\right) \quad (2\text{-}16)$$

Where:

β_w= correction factor for wall slip (m^3/Ns)

Including all three of these terms in equation (2-9) gives the amended L-W equation proposed by Gardner et al. (2012) (2-17)

$$p_{c0}(1 - \beta_s) - \frac{2\beta_m\dot{z}}{r} - \rho g z \sin\varphi - \frac{z}{\left(\frac{r\beta_w}{2} + \frac{r^2}{8\mu}\right)}\dot{z} = 0 \quad (2\text{-}17)$$

This equation is also useful for modelling planar cracks, although in this case, the radius of the capillary tube, r, is replaced by the crack width, b and the effective permeability term takes the value k=b^2 /12.

In the case represented in Figure 2.8 b) of non-uniform capillary, Young (2004) explain the change in fluid velocity relating this one with the speed of the fluid front by applying the conservation of mass:

$$\dot{z}A(z) = v(x)A(x) \qquad (2\text{-}18)$$

Where:

A(x) = cross-section area of the capillary

A(z) = cross- sectional area at the meniscus interface.

Applying the same principles to equation 2-11 and rearranging gives the following equation for flow in non-uniform capillaries:

$$\dot{z} = \frac{p_{c0}(1-\beta_s) - \rho g z \sin\varphi}{\frac{2\beta_m}{r(z)} + \eta} \qquad (2\text{-}19)$$

in which

$$\eta = A(z)\int_0^z \frac{1}{\left(\frac{r(x)\beta_w}{2} + \frac{k(x)}{\mu}\right)A(x)}\,dx \qquad (2\text{-}20)$$

Where the term η represents the total viscous resistance to flow (Ns/m^3)

To make sure that the time of fluid flow is found, an initial value of z needs to be chosen, and therefore η can be evaluated using a direct integration time stepping procedure.

This numerical response can be checked against the analytical expression given by Fries and Dreyer (2008) that is expressed in the equation 2-21

$$h(t) = \frac{a}{b}\left[1 + w\left(-e^{-1-\frac{b^2 t}{a}}\right)\right] \qquad (2\text{-}21)$$

Where:

$$a = \frac{\sigma r \cos\theta}{4\mu} \cong \frac{2\sigma\cos\theta}{\phi\mu}\cdot\frac{k}{R} \qquad (2\text{-}22)$$

$$b = \frac{\rho g r^2 \sin\varphi}{8\mu} \cong \frac{\rho k g \sin\varphi}{\phi\mu}\cdot\frac{k}{R} \qquad (2\text{-}23)$$

w = Lambert function W(x)

2.10 Summary of the relevant previous work

A lot of studies about capillary flow in porous media have been conducted in the last years, but only few of them are focused on flow in discrete cracks.

Roels et al. (2003) studied the capillary flow in a discrete crack surrounded by a porous matrix media using a numerical model that solved a combination of a quasi static pressure equation with a Darcian flux equation, and verified the results with experimental data. The team of researches confirmed that when the crack aperture is 0,1 mm or superior absorption by the surroundings did not exist and thence, the matrix can be neglected because it does not affect the capillary rise in the crack (Roels et al. 2003 and Carmeliet et al. 2004).

Gardner et al. (2012) investigated both experimentally and numerically the influence of the crack aperture, the age of the specimen and the mortar saturation in the capillary rise of water in discrete cracks with apertures from 0,094 to 1,170 mm and different crack configurations (planar, four-stage sloped and natural) in mortar. They reported a lower final rise height with the increasing of the crack width and also in the natural configuration compared with the others, and a slower rate of the capillary rise in the older samples (28 days against 7 days) and in the saturate specimens. Furthermore, they were able to model successfully the flow with an amended Lucas-Washburn equation, and in the same study, they proposed a function that related an equivalent planar opening with a mean aperture of a natural crack (Equation 3), but suggested that further research should be necessary in order to clarify the limit and the shape of the function.

Finally, Gardner et al. (2014) conducted a new study similar to the previous one but using cyanoacrylate as a healing agent, and they analysed its influence.
To sum up, the observations revealed by Roels et al. (2003) and the previous work conducted by the Dr. Gardner team at Cardiff University forms the starting point of the present investigation.

3 EXPERIMENTAL PROCEDURE

In this section methodology are outlined together with the design of the experimental procedures.

3.1 Materials

The cement used was CEMII/B-V32,5R supplied by Lafarge and manufactured to conform to BS EN 197-1:2000. The fine aggregate component of the mix consisted of sea-dredged sand from the Bristol Channel, conforming to BS EN 12620:2002. Particle size distribution tests according to BS EN 933-1:1997 were performed to establish the gradation of the sand..

The sample size selected was fine aggregate consisting in concreting sand with a maximum particle size of 4 mm, and coarse aggregate with a maximum particle size of 10 mm (BS EN 12620:2002).

The mix proportions were selected proportions in order to obtain the compressive strength of C20, C30 and C50 N/mm^2. The composition of the concrete mixes can be seen in Appendix A.

3.2 Specimen manufacture

In the case of the artificial (planar) crack, the specimens have already existed and were cast one year ago. Seven pairs of 25 x 50 x 300 mm (W x L x H) prisms (2 for the C20, 2 for C30 and 3 for the C50) were used in order to form, with the help of different sizes of spacers, crack apertures between 0,1 and 0,3 mm. In the appendix C is shown the specimens numbers and the different crack apertures performed in any of them. Note that for carry out the 7-day-old experiments there were nine pairs of prisms, but two of them were lost in the laboratory.

On the other hand, in order to obtain the specimens for the natural crack configuration 24 prisms of 75 x 75 x 255 mm were cast, 2 for each crack width (0.5, 1.0, 1.5 and 2.0 mm) in each concrete (C20, C30 C50).

In both configurations, 3 cubes of 100 x 100 x 100 mm from each of the previous mixtures were cast additionally and tested after 7 days in a cube compression test to obtain the compressive strength (Appendix B)

Typically 3 tests were performed for each crack width for all crack

configurations, specimen ages and concrete strength. An exact breakdown of the number of specimens tested is provided in appendixes C and D.

3.3 Casting

For all the natural configuration mixes the following mixing procedure was used:

The dry constituents materials, sand and cement, were weighed in buckets to an accuracy of 0,05 kg and added to a Cumflow horizontal pan mixer with a capacity of approximately 250 kg. They were dry mixed together for approximately two minutes before half of the water was added slowly using a visual inspection of the mix to achieve a suitable workability. The mixer was stopped and the mix was manually mixed to get dry unmixed material out from the corners. The remaining water was added slowly whilst mixing and the manual mix was repeated. After a final two minutes of mixing the mortar was ready to be cast, and then the mixture was placed into the moulds.

The figures 3-1 and 3-2 show the vibrating table, the mixer and the moulds.

Figure 3-1. Vibrating table and Cumflow horizontal pan mixer used in the casting procedure of the natural crack configuration

Figure 3-2. Moulds used in the casting procedure of the natural crack configuration

The moulds were filled in thirds. After each third was added the moulds were vibrated for 30 seconds on a vibrating table. This process was repeated for the remaining two thirds of the moulds. Once all of the mortar was placed in the moulds, the tops were levelled using a pallet knife.

3.4 Specimen curing and prisms preparation

In the case on the artificial (planar) configuration, the specimens were cured and cut in order to create the prisms of 25 x 50 x 300 mm one year ago, and stored in the laboratory at room temperature during this time.

On the other hand, the natural configuration specimens were cured in water for seven days. Later, the 75 x 75 x 255 mm beams were loaded until failure in a three point bending test in order to create the natural crack.

The three point bending tests were carried out using a load cell, transducer and hydraulic loading machine. The beams were loaded with a central point load and supported on rollers 200 mm apart. Previously, the specimens has been central notched with a 5 mm notch such that cracking was initiated in the centre of the specimen and to encourage a near vertical crack path. The load was applied at the midpoint between the two supports until the failure of the beam as it can be seen in figure 3-3.

Figure 3-3. Three point bending test used to create the natural crack specimens.

Once the prisms were fully cracked a pair of 25 x 75 x 75 mm bits were cut off from the central part of the cracked beam using a circular concrete cutting saw and the resultant pieces were used to create the crack widths between 0,5 and 2 mm.

3.5 Measurement of the concrete strength

The compressive strength was obtained doing cube compression test. The cube specimens were tested in compression to the method in BS EN 12390-3:2009. Each cube was loaded into the cube crushing apparatus with 100x100 mm steel plates top and bottom. The specimens were positioned such that the direction of loading was perpendicular to the casting direction as can be seen in figure 3-4.

The applied load was increased at a rate of 360 kN/min until no further load increase could be sustained. The specimens were then unloaded and removed from the apparatus. The peak load in kN was recorded as the failure load.

After failure of each cube the specimen was examined. The failure mode was compared with the acceptable and unacceptable failure patterns in BS EN 12390-3:2009 shown in appendix B. The compressive strength of each test was recorded and the values obtained are showed in the appendix B.

Figure 3-4. Cube compression test used

3.6 Crack configurations and apertures

A range of crack apertures were achieved in artificial (planar) and natural configurations both with short lengths of steel, nickel or tin wires with diameters varying from 0,1 to 2 mm. The diameters of the wires were measured using a vernier caliper over various positions along a piece of the wire. The apertures created were then measured with a portable crack width microscope and the actual crack aperture recorded.

For the planar and the natural configurations experiments wires of a constant diameter were placed between the two specimens at the bottom, middle and top of the specimens. The ensemble was then clamped together to keep the wires in place.

3.7 Flow agent

The fluid that was used as flow agent in the experiments was tap water at room temperature (20°C). Its physical parameters were:

- Surface tension: γ = 0,0728 N/m.
- Dynamic viscosity: μ= 0,001221 Ns/m^2.
- Density: ρ = 1000 kg/m^3

The contact angle between the concrete and the water was also measured because is a fundamental element of the equation of capillary flow. The contact angle was examined via the sessile drop technique. This technique was performed at regular intervals over a period of 1 hour, and the contact angle between the drop and the solid surface and the profile of the surface was obtained using ImageJ with a DropSnake plug-in developed by Stalder et al. (2006). The value obtained were:

- liquid/solid contact angle: $\theta = 22{,}8^{o}$

3.8 Experimental equipment

3.8.1 High speed camera

High-speed video cameras are an excellent tool for capturing a moving process at an accelerated rate.

An AOS MOTIONeer high-speed video camera have been selected for these particular experiments. This camera can record up to 32,000 frames a second which allowed the rise height of the fluid through the crack to be recorded and then replayed at a slower rate for data processing purposes.

In order to capture the full rise height of the fluid the experiments were recorded at 250 frames per second. This was chosen as a valid parameter in previous researches presented in chapter 2: literature review.

3.8.2 Lighning

Lighting was required in order to gain clear visibility through the simulated cracks. Two spot lights were used to illuminate the front of the specimens so that the laminated scale could be seen on the camera, and two low intensity back halogen lights, with adjustable intensity were placed directly behind the specimens to illuminate the crack. The larger the crack size, the less light was needed, therefore the lights behind the crack were adjusted in response to this. Lighting in the experimental work looking at natural cracks was a particular challenge due to the tortuosity of the crack in two dimensions and therefore there was difficulty in shining the light provided by the halogen lamp through the entire crack plane.

3.9 Experimental set-up

The experimental set-up is shown in figures 3-5 to 3-9. The wires were placed onto the specimens and then they were clamped together (as discussed previously), and a petri dish with the water was lifted to the underside of the plates using a hydraulic pump.

A scaled piece of laminated graph paper was used as the measurement tool for looking at the overall capillary rise height within the specimen. This method allows rise height to an accuracy of 0.5mm to be measured. The rise height with respect to the rise time was then obtained. Capillary flow was measured with the high-speed camera placed at 150 mm over a total time of 90 seconds which includes the addition of the water to the petri dish.

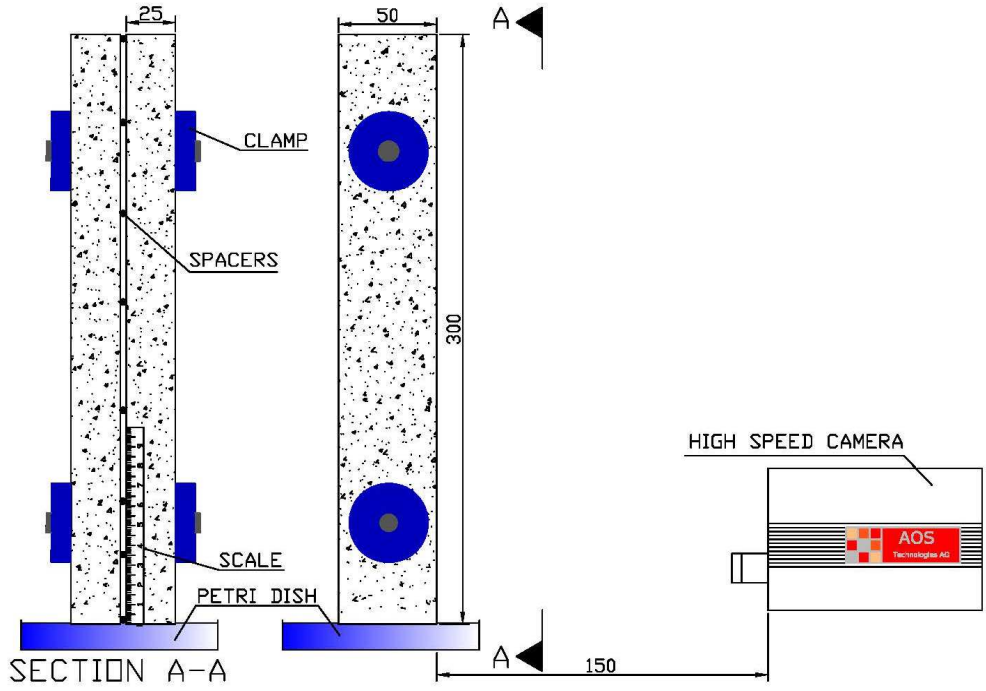

Figure 3-5. Configuration of the experiment for the planar crack. Dimensions in mm

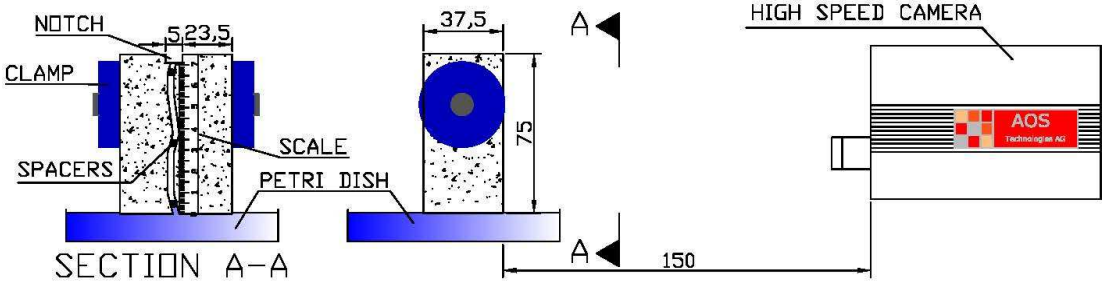

Figure 3-6. Configuration of the experiment for the natural crack. Dimensions in mm

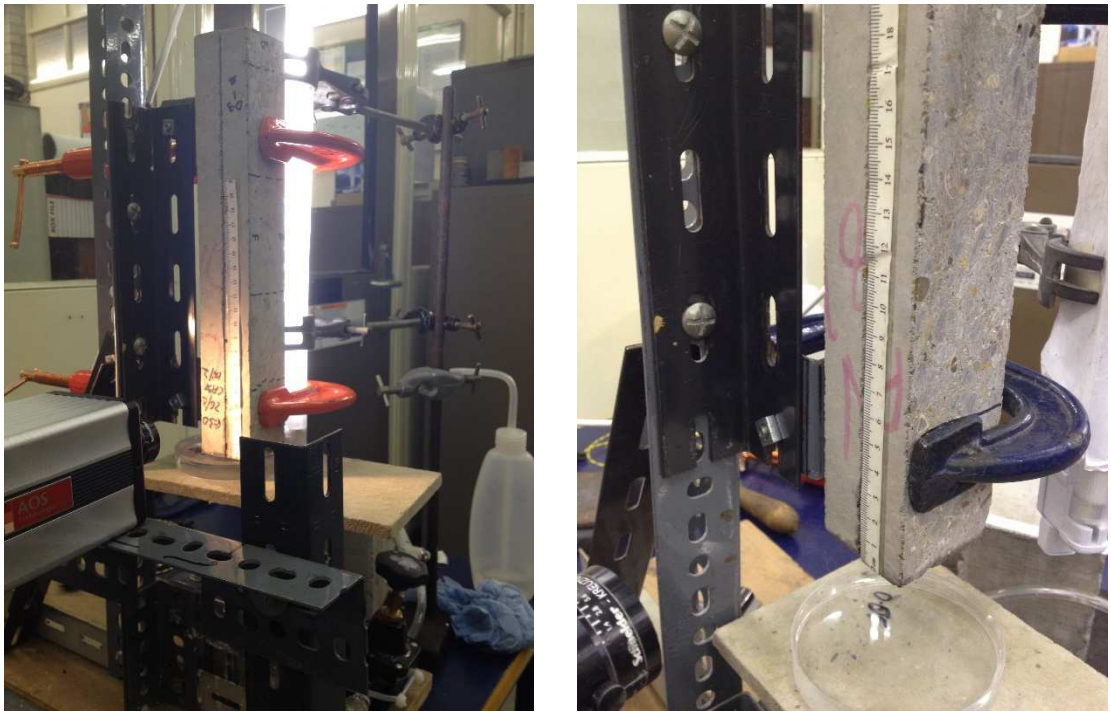

Figure 3-7. Configuration of the experiment for the planar crack

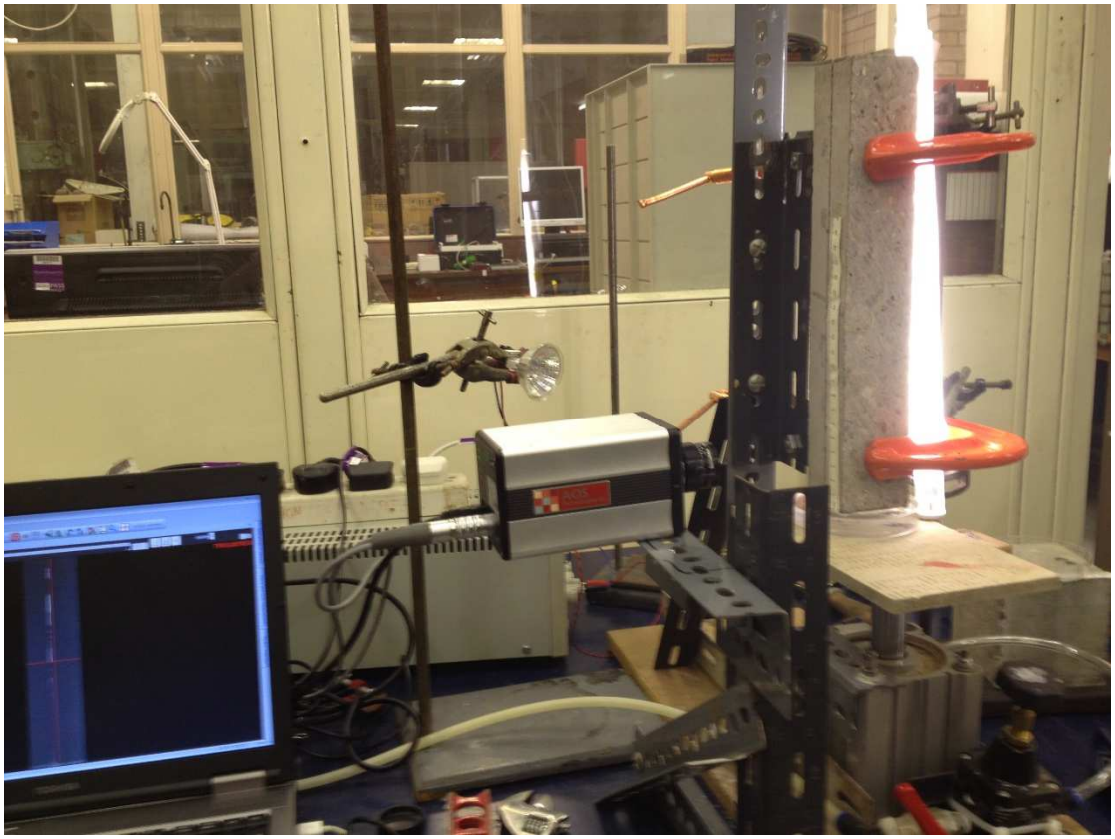

Figure 3-8. Configuration of the experiment for the planar crack

Figure 3-9. Configuration of the experiment for the natural crack

3.10 Data processing

As there were a total of 22.500 frames for each video clip, only the frames showing the movement of the fluid in the crack were retained. The end of capillary flow was taken as the point where no further rise height occurred with time. The reason for this is that it is the initial stages of capillary flow that are of importance, particularly in autonomic healing when there is a high potential for rapid hardening of the healing agents and therefore, even though there will be further capillary rise over time, it is the first few seconds that are of interest.

4 EXPERIMENTAL RESULTS AND DISCUSSIONS

This chapter considers the results from the experimental work undertaken in the laboratory. The experimental results can be considered in two distinct sections. The first section is relative to the artificial planar cracks, where three different characteristics of the capillary rise response of water in concrete will be analysed: The effect of crack width, the effect of concrete strength, and the effect of specimen age.

Secondly, the natural crack configuration will be studied in order to adjust a new function that relates the natural crack width with an equivalent planar aperture.

The majority of the experiments were performed in triplicate and therefore, due to the substantial quantity of data available, only the average result from the experiments or the most coherent of them has generally been selected and presented in this chapter. However, all results are given in Appendix C and D.

All data has been extracted from experimental videos. Capturing the data over a short period of time enables us to look at the immediate capillary rise response of the system giving an indication of the ability and velocity of a flow agent to move through a discrete crack. The figure 4-1 shows how the capillary rise in planar cracks looks in the videos and in the figure 4-2 are displayed the specimens at the end of the experimental procedure.

For the natural crack configuration, only the equilibrium final height was extracted due to it is not necessary for adjust the planar equivalence function to have the complete sequence of the capillary flow response. The figure 4-3 shows how the capillary rise in natural cracks looks in the videos and the figure 4-4 displays the specimens at the end of the experimental procedure.

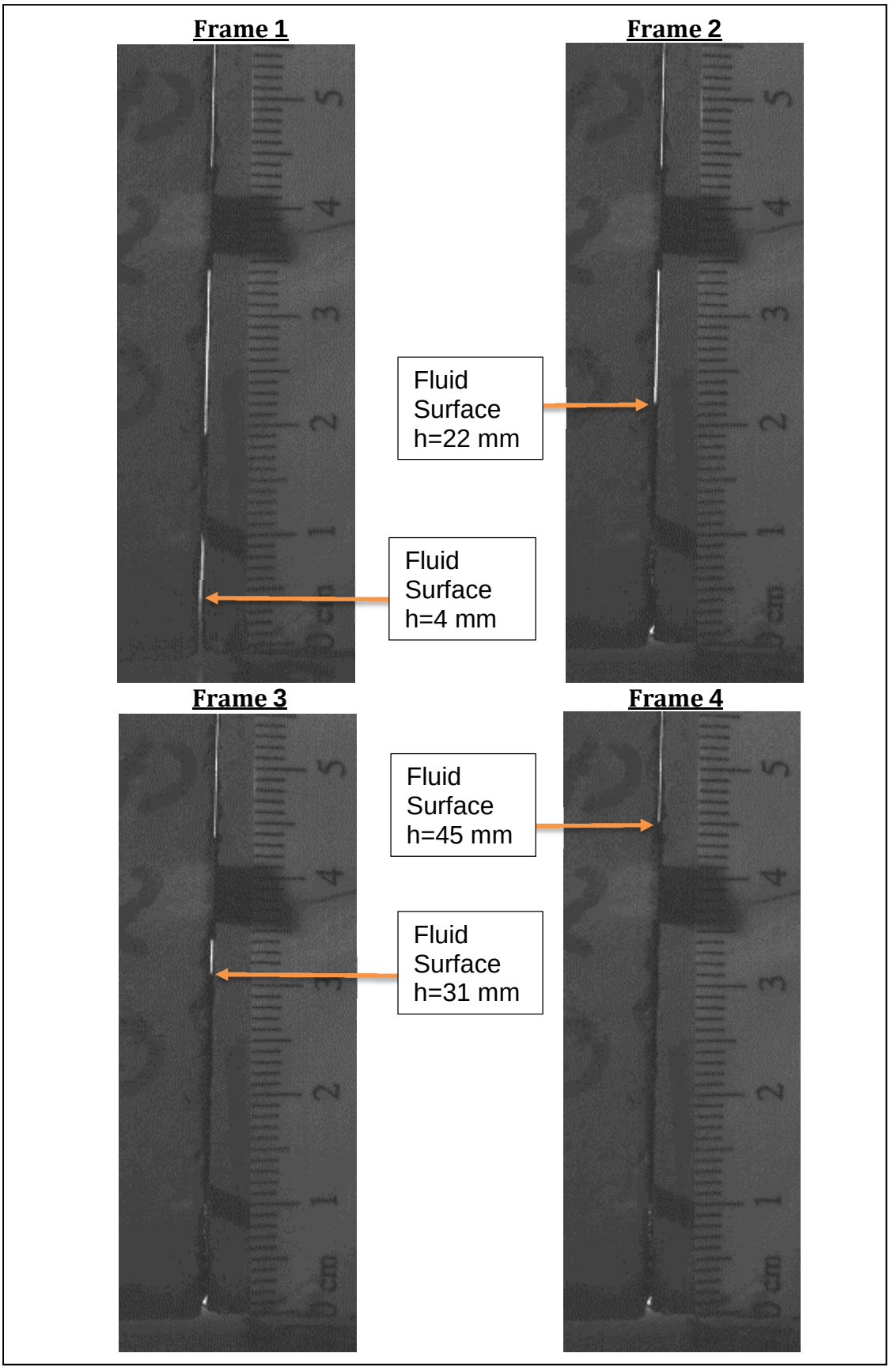

Figure 4-1 Example of extraction the capillary rise response in a planar crack from video sequence.

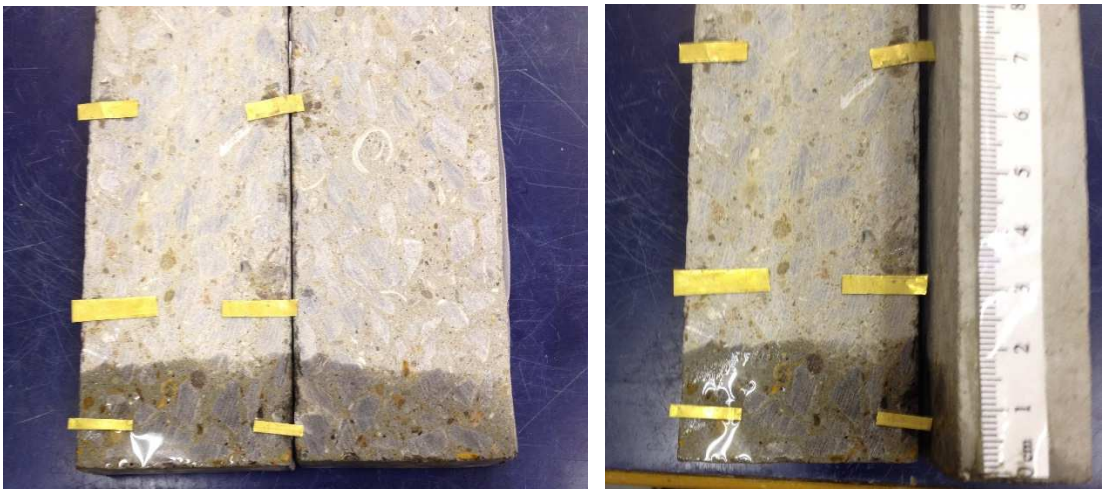

Figure 4-2. Example of planar crack specimens at the end of the experimental procedure

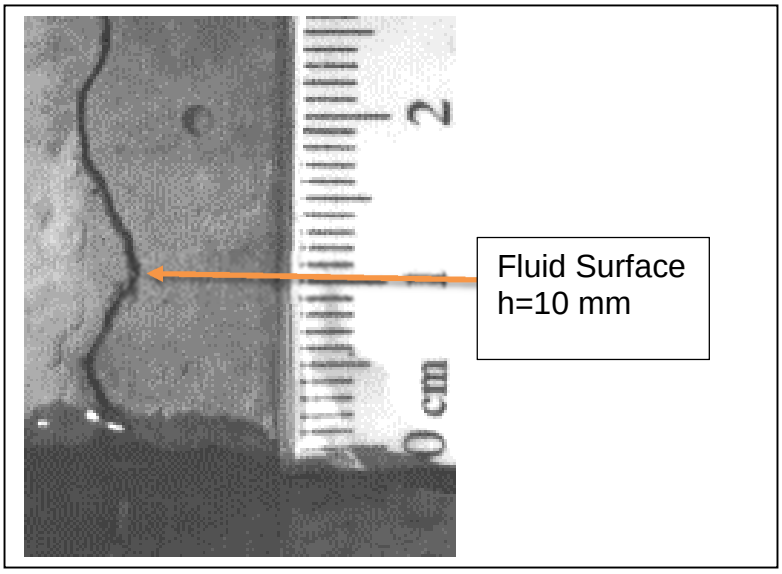

Figure 4-3. Example of extraction the equilibrium capillary rise height in a natural crack from video sequence.

Figure 4-4. Example of natural crack specimens at the end of the experimental procedure

4.1 Effect of crack width

The effect of crack width is widely studied in mortar by the previous works as it can be seen in the chapter 2. Literature review section. However, it is interesting show here the general behaviour of the capillary flow in the case of concrete, and explain the source of possible mistakes in the results.

The figures 4-5 to 4-8 show the capillary rise response for flow in different planar crack apertures.

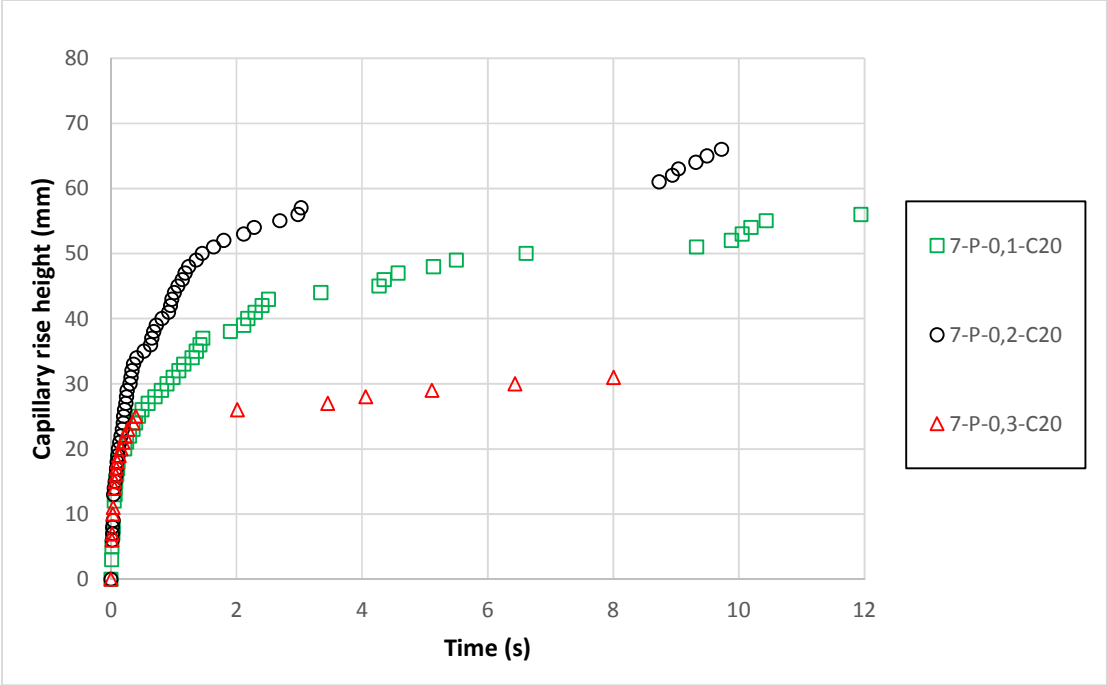

Figure 4-5. Capillary rise response in planar cracks of 0,1 mm, 0,2 mm and 0,3 mm for C20 concrete specimens

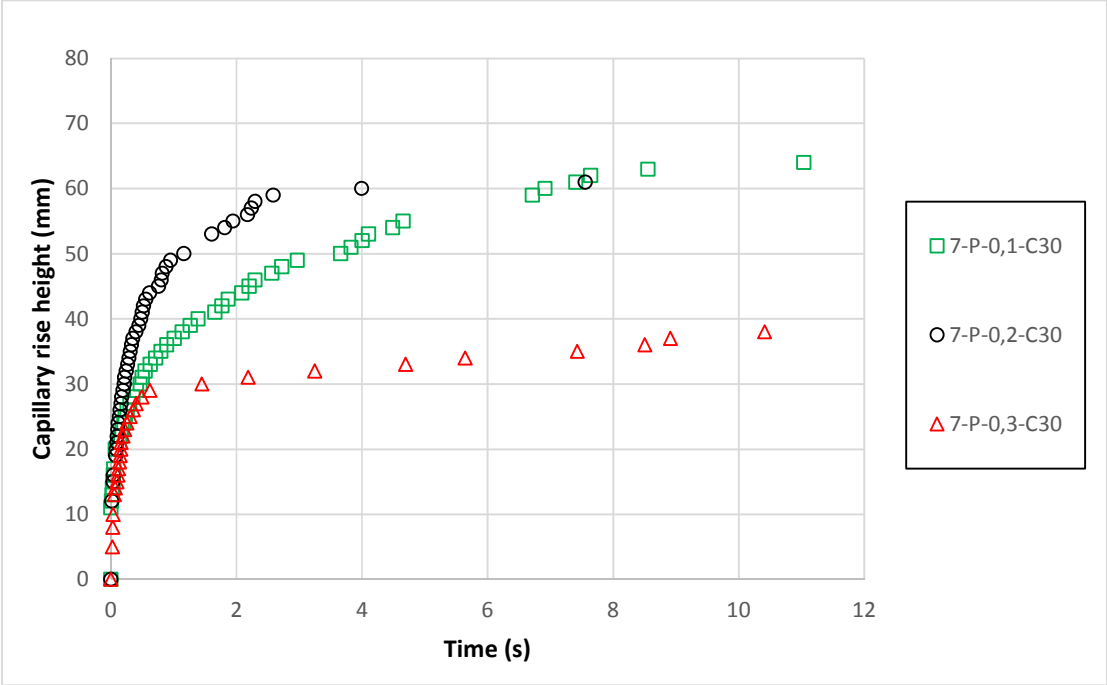

Figure 4-6. Capillary rise response in planar cracks of 0,1 mm, 0,2 mm and 0,3 mm for C30 concrete specimens

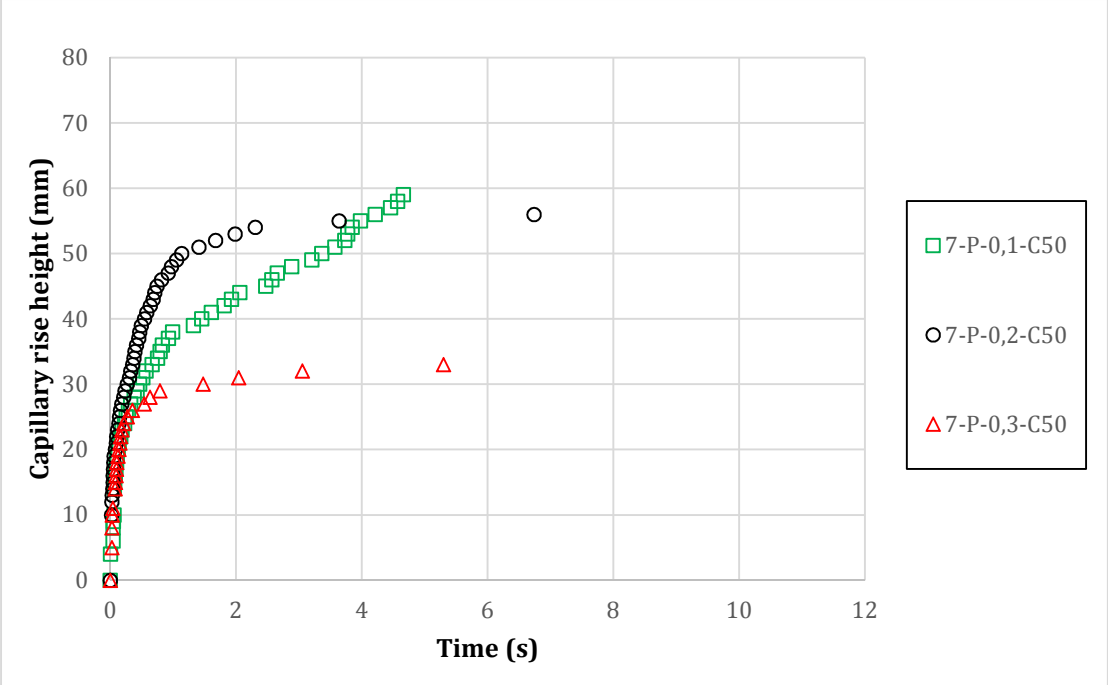

Figure 4-7. Capillary rise response in planar cracks of 0,1 mm, 0,2 mm and 0,3 mm for C50 concrete specimens

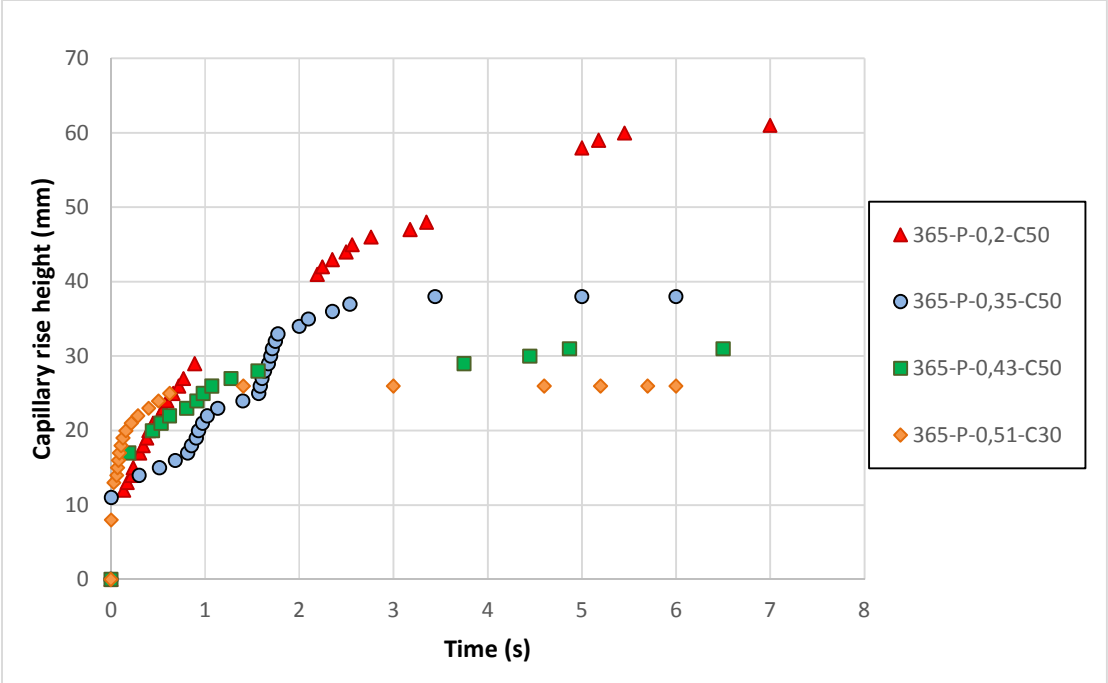

Figure 4-8. Capillary rise response in planar cracks of 0,2 mm, 0,35 mm, 0,43 mm and 0,51 mm for C50 and C30 concrete specimens

The experiments shown in figures 4-5 to 4-8 have consistency with the theory of the Lucas-Washburn equation that the wider the crack aperture of the capillary the lower the equilibrium capillary rise height (equation 2-11).

However, we can observed in several figures that in the crack apertures of 0,1 mm, the equilibrium capillary rise height is almost the same or even lower than the 0,2 mm apertures. One of the reasons for this, as it was explained in Hoffman (2012), may be attributed to the actual crack width is larger than that suggested by the thickness of the wire used and furthermore, the protrusion of particles on the surface causing blockages of the flow path. Figure 4-9 shows an example of the real crack width measured from a video image. In this figure it is shown that for an assumed crack aperture of 0,1 mm measurements of actual crack apertures range from 0,08 mm to 0,23 mm. This is due to variations of the concrete faces caused through the manufacture of the specimens and achieving a uniform clamping force over the height of the specimen. It should be noted that the variable brightness of the lamp behind the specimens is responsible for the impression of a wider aperture than that reported.

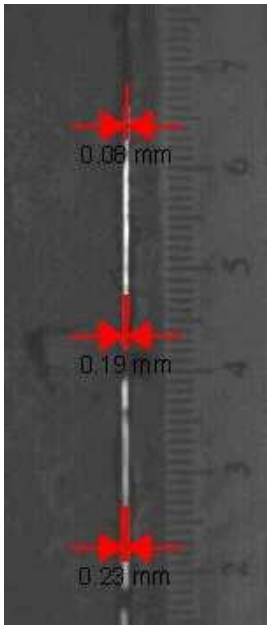

Figure 4-9. Measured crack apertures for a crack width of 0,1 mm

Consequently, there was some variation in the actual crack apertures used in the experiments which would influence the magnitude of the variation in the results. Although, this effect will be apparent in the majority of the tests it has a greater effect on the capillary rise heights in the narrower capillaries. This is

why the final rise height is sometimes even lower than the measured equilibrium rise height of 0,2 mm. Therefore, when analysing the data it is important to understand what the actual crack aperture was to determine the capillary flow.

4.2 Effect of concrete strength

Three different concrete strengths, C20, C30 and C50, were examined as part of the experimental work in this thesis. This section looks at how a change in concrete strength affects capillary flow through discrete fractures in concrete.

In order to get a better comparison and dismiss other sources of influence in the capillary rise, only the 7-days specimens will be compared. This is because the availability of data from the younger samples is higher due to, as can see in the appendix C, some prisms were lost in the laboratory and consequently it was not possible reproduce in the older specimens all the experiments in the whole crack apertures.

All concrete strength are graphically compared in the figures 4-10 to 4-13 in order to try and determine relationships between them from the rise heights responses.

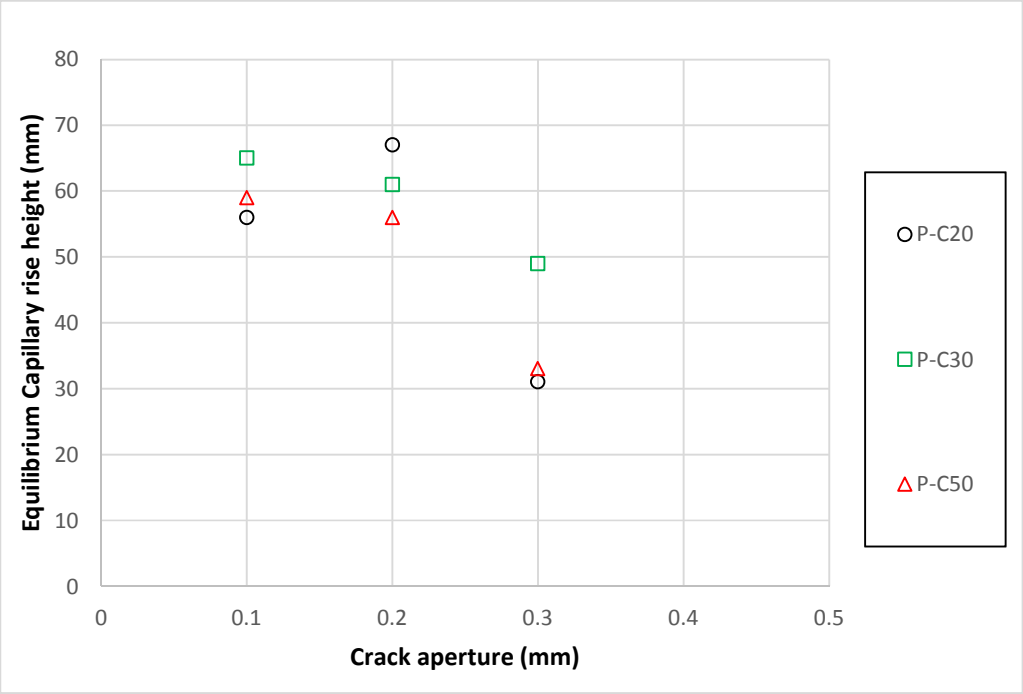

Figure 4-10. Planar crack final capillary rise height for C20, C30 and C50 concrete strength specimens

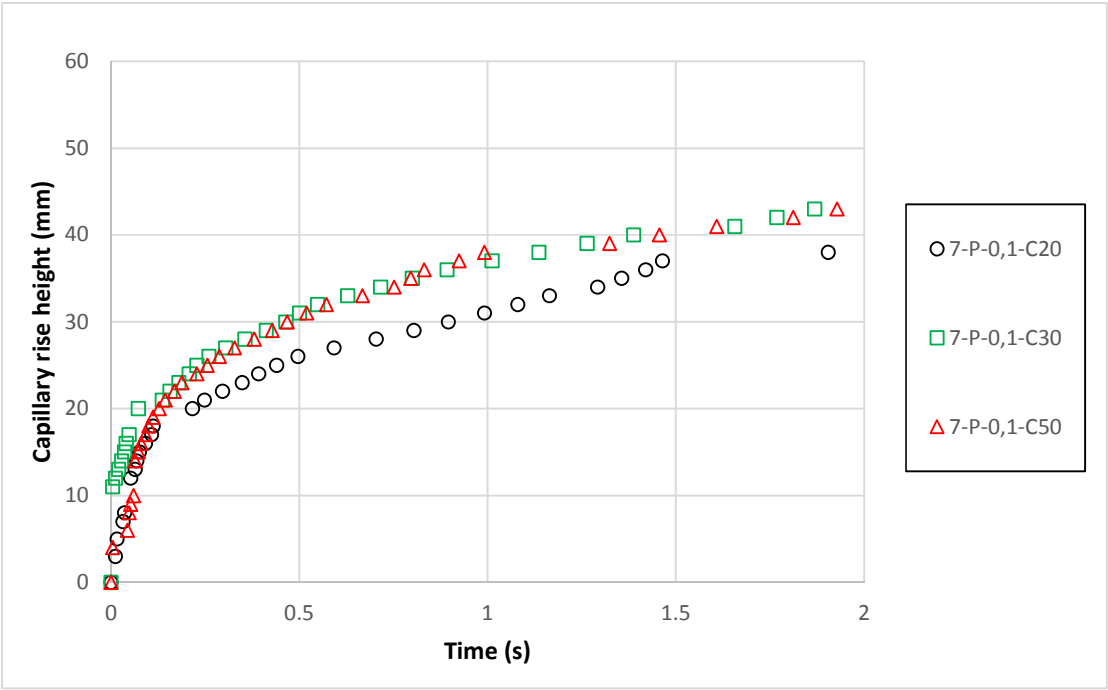

Figure 4-11. Capillary rise response in planar cracks of 0,1 mm for C20, C30 and C50 concrete strength specimens

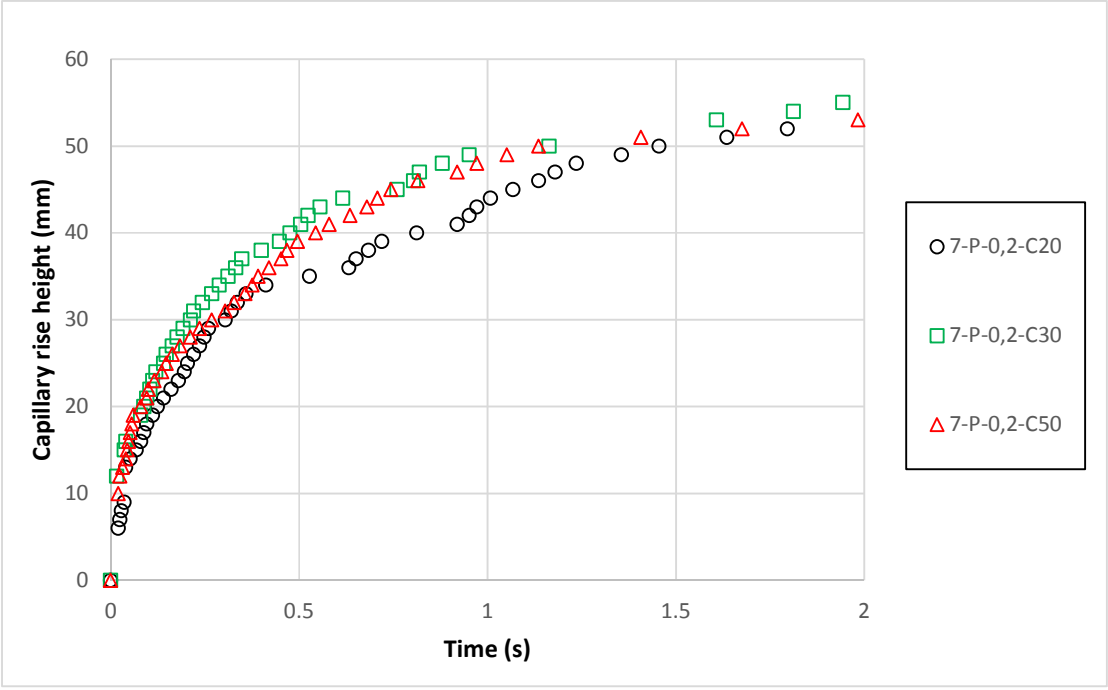

Figure 4-12. Capillary rise response in planar cracks of 0,2 mm for C20, C30 and C50 concrete strength specimens

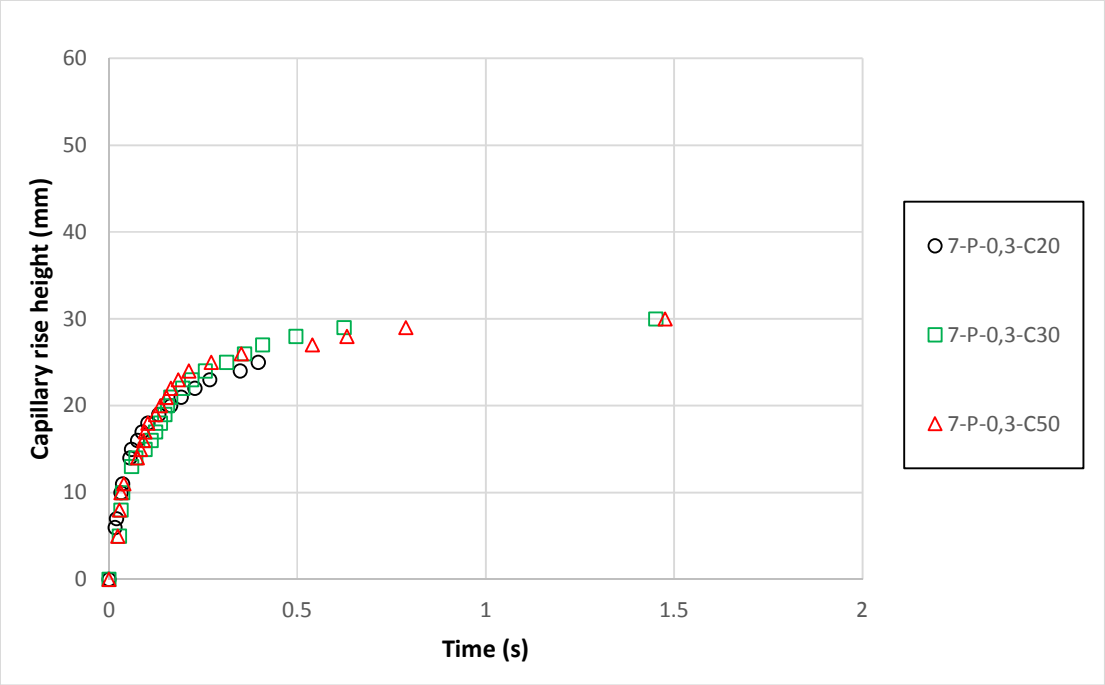

Figure 4-13. Capillary rise response in planar cracks of 0,3 mm for C20, C30 and C50 concrete strength specimens

Results in figure 4-10 displays that there is no a clear relationship between the final rise heights for the C20, C30 and C50 specimens. Also, in some cases, water with the same crack aperture of 0,1 has a lower rise height than 0,2. This is due to the same reasons as described in previous section where the crack aperture effect is evaluated.

On the other hand, looking at figures 4-11 to 4-13 it can be seen that there is no significant difference between the results for the specimens, although the rate of rise is slightly slower with the C20 mixture compared to C30 and C50, where it is almost the same.

Consequently, it could be assumed that the concrete strength does not affect the capillary rise response although without further measurements this is difficult to ensure because the results have been inconclusive.

4.3 Effect of specimen age

The effect of the concrete age in the capillary flow of water was evaluated via the comparison of old 1-year planar water tests with young 7-day planar water tests.

Looking at this specific parameter can give an idea of the ability of the healing agent to flow in both young and mature cementitious matrices, hence indicating the potential for healing to occur in cracks formed at early age, due to shrinkage and early thermal effects and those formed at later stages as a result of load application or deterioration processes.

In this case, the effect of the specimen age is discussed for the 0,2 mm crack aperture only, because the 0,1 mm crack width does not reach its theoretical value as it was proved in the previous chapter, and the crack aperture of 0,3 mm have a very fast initial rise response that produce in same cases absence of capillary rise data for rise heights of less than 1 cm.

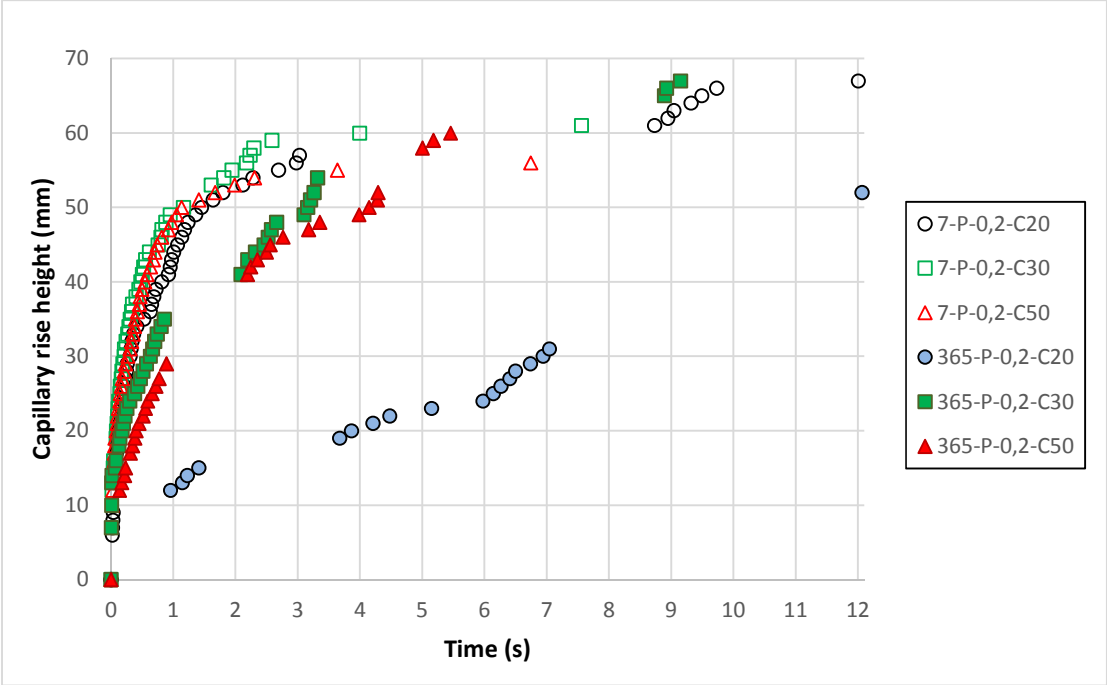

Figure 4-14. Capillary rise response in planar cracks of 0,2 mm for 7 and 365-day-old in C20, C30 and C50 concrete strength specimens

In the figure 4-14, the retardation of the fluid for old, 0,2 mm, C20 strength is as a result of the wire restricting the flow of the fluid in the discrete crack. Thus, the wire acted as a blockage in the flow path and therefore this result are not considered in the following discussion.

The results show that at the end of the experiments, the water reached a very similar equilibrium height in all the cases, although the rate of capillary rise in the mature specimen was much slower. This observation is consistent with the

previously reported for the capillary flow of water in 28-days old planar cracks by Gardner et al. (2012).

This difference between the rise response of young and old specimens may be attributed to the effect of the time dependent development of the mortar microstructure wall surface on the dynamic resistive forces acting during capillary rise.

4.4 Natural crack configuration and planar equivalent function

An investigation into the effect of concrete strength on the final capillary rise height in natural discrete cracks in cementitious materials has been examined in this section together with the adjust of the function that relates the natural crack aperture with an equivalent planar crack width described by the equation 3 in the chapter 2. Literature review.

C20, C30 and C50 concrete mixtures have similar overall rise heights in all the crack apertures considered as can be confirmed in figure 4-15, and do not follow a specific pattern. The differences between the values at the same crack aperture may be produce by the different tortuosity of the crack. Therefore, the concrete strength does not affect the final rise height in the natural configurations.

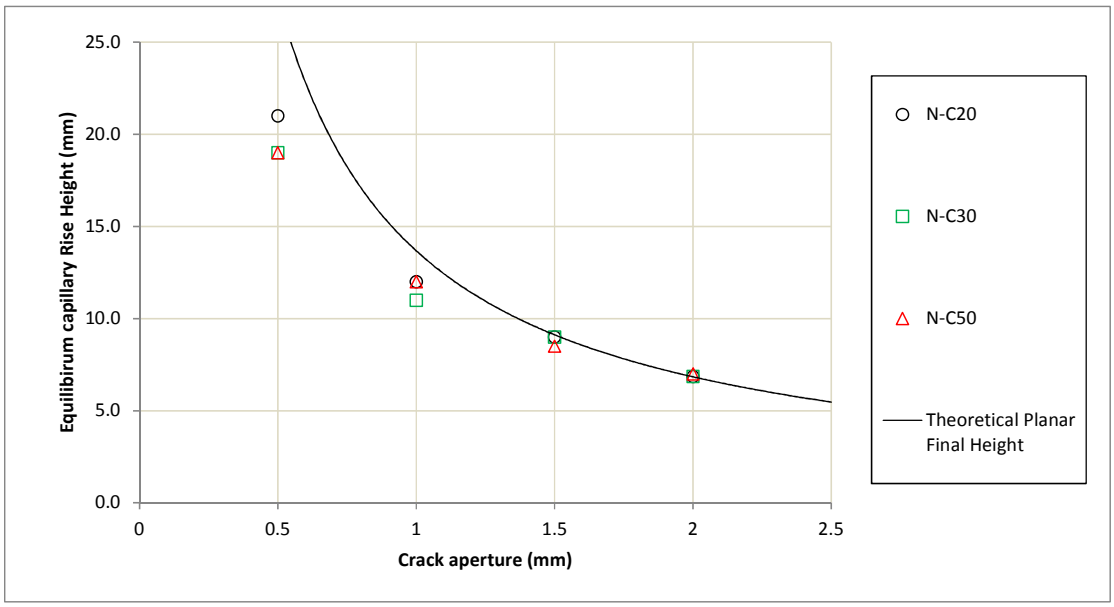

Figure 4-15. Comparison of final capillary rise height of natural crack aperture for C20, C30 and C50 specimens and with theoretical planar final height data

Also, it can be seen in the figure 4-15, that there is a close match between the numerical and experimental capillary final rise in the wider crack apertures. This is consistent with the definition by Gardner et al (2012) of a threshold value of the crack aperture above which the capillary rise response for the planar and the natural crack is the same (C_{we}) and the influence of the relative roughness in the natural crack in proportion with the fracture width is negligible.

In the figure 4-16, it is showed the capillary rise final height for an equivalent planar crack compared to the experimental natural crack configuration, and the Planar Equivalence Function adjusted for concrete and created using wider crack openings (0,5, 1, 1,5 and 2 mm).The used values are shown in table 4-1.

The Planar Equivalence Function is described by equation 3 in the Chapter 2. Literature Review, and the value of the parameters that better fit with the concrete specimens data are: k_0 = 2; k_m= 1; C_{we} = 2 and n = 3. It can be observed that the new Planar Equivalence Function for concrete differs from the one of mortar drawn by Gardner et al. 2012, where the value of the parameters were k_0 = 4; k_m= 1; C_{we} = 2 and n = 6. However, the C_{we} still the same in this new study with wider crack apertures, confirming that the limit established previously by the authors (2 mm) was accurate.

	Natural Crack (mm)	**Natural Final Height (mm)**	**Planar Crack equivalent (mm)**
C20	0,5	21,0	0,65
C20	1	12,0	1,14
C20	1,5	9,0	1,52
C20	2	6,9	2,00
C30	0,5	19,0	0,72
C30	1	11,0	1,24
C30	1,5	9,0	1,52
C30	2	6,9	2,00
C50	0,5	19,0	0,72
C50	1	12,0	1,14
C50	1,5	8,5	1,61
C50	2	7,0	1,95

Table 4-1 Equilibrium rise height in natural configuration and planar crack equivalent aperture

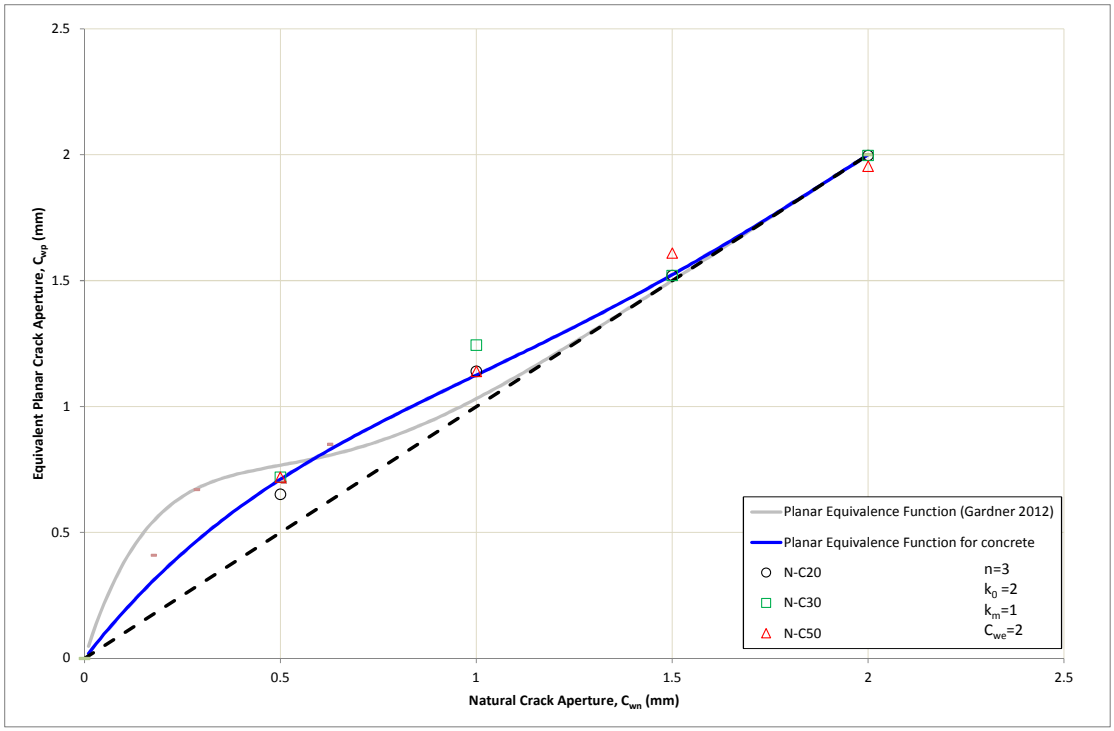

Figure 4-16. Function that relate an equivalent planar opening with a mean aperture of a natural crack adjusted for concrete mixtures and compared with the original by Gardner et al. (2012)

5 NUMERICAL SIMULATION OF CAPILLARY FLOW

In this section, comparisons are made between a selection of the results from experiments described in section 4 and the results obtained from the amended Lucas–Washburn equation (2-17) derived in section 2.

The experimental results presented examine the effect in the capillary rise response of crack aperture and concrete age in planar discrete cracks.

The equation 2-17 is solved using an explicit integration time-stepping procedure and a check is undertaken to ensure that the time step is sufficiently small to give converged results.

Specifically, the solutions presented used a time step size of 0,0001 s and if reduced to 0,00005 s the predicted responses would be indistinguishable from each other on the numerical simulations shown.

The appendix E presents the numerical solution of the capillary rise equation write in Mathcad v.15 code with all the parameters used. The physical parameters of the fluid used to simulate the experimentally observed capillary rise are the same that are described in section 3.7.

5.1 Effect of correction parameters

Each of the correction factors in in the amended Lucas–Washburn equation (2-17) has a distinct influence on the shape of the capillary rise response:

1- β_s= Correction factor for stick–slip behavior at the moving front

An increase in β_s, produces a lower equilibrium rise height and also a fall at the rise rate.

2- β_m= Correction factor for frictional dissipation at the meniscus front

The parameter β_m retard the capillary rise rate and it was find in previous researches that it is independence of any combination of fluid/solid.

3- β_w= Correction factor for wall slip

The correction β_w should accelerate the capillary rise rate as a result of the decreased net resistance to flow.

In the table 5.1 it is summarised the published correction parameters

Reference	2012 (1) (2)	2012 (1) (2)	2012 (1)	2012 (1)	2014 (3)	2014 (3)	2014 (3)
Flow agent	Water	Ethil	Water (4)	Water (4)	Cyanoac. (5)	Cyanoac. (5)	Cyanoac. (5)
Medium	Glass d = 0,57 mm	Glass d = 0.57 mm	Glass d = 0.2 , 0.5, 1 mm	Mortar P 28 days	Glass d = 0,2, 1 mm	Mortar P_I_Ta 7 days	Mortar P_I_Ta 28 days
β_s **(-)**	0,01	0,01	0,35	0,01	0,01	0,12	0,01
β_m**(Ns/m²)**	0,22	0,07	0,35	0,55	0,08	0,35	0,35
β_w **(m³/Ns)**	0	0	0	0	0	0	0

Notes:

(1) From Gardner et al 2012.

(2) Capillary rise data from Legrande et al (1945)

(3) From Gardner et al 2014

(4) Water properties: Equilibrium contact angle (θ_0)= 0º Surface tension (γ) = 0,0728 N/m

(5) Cyanoacrylate properties: Equilibrium contact angle (θ_0)= 10º Surface tension (γ) = 0,033 N/m

P =Planar ; I =Inclined; Ta = Tapered

Table 5-1. Summary of the published correction parameters

In the figure 5-1, it can be seen the magnitude of the modification of the correction parameters.

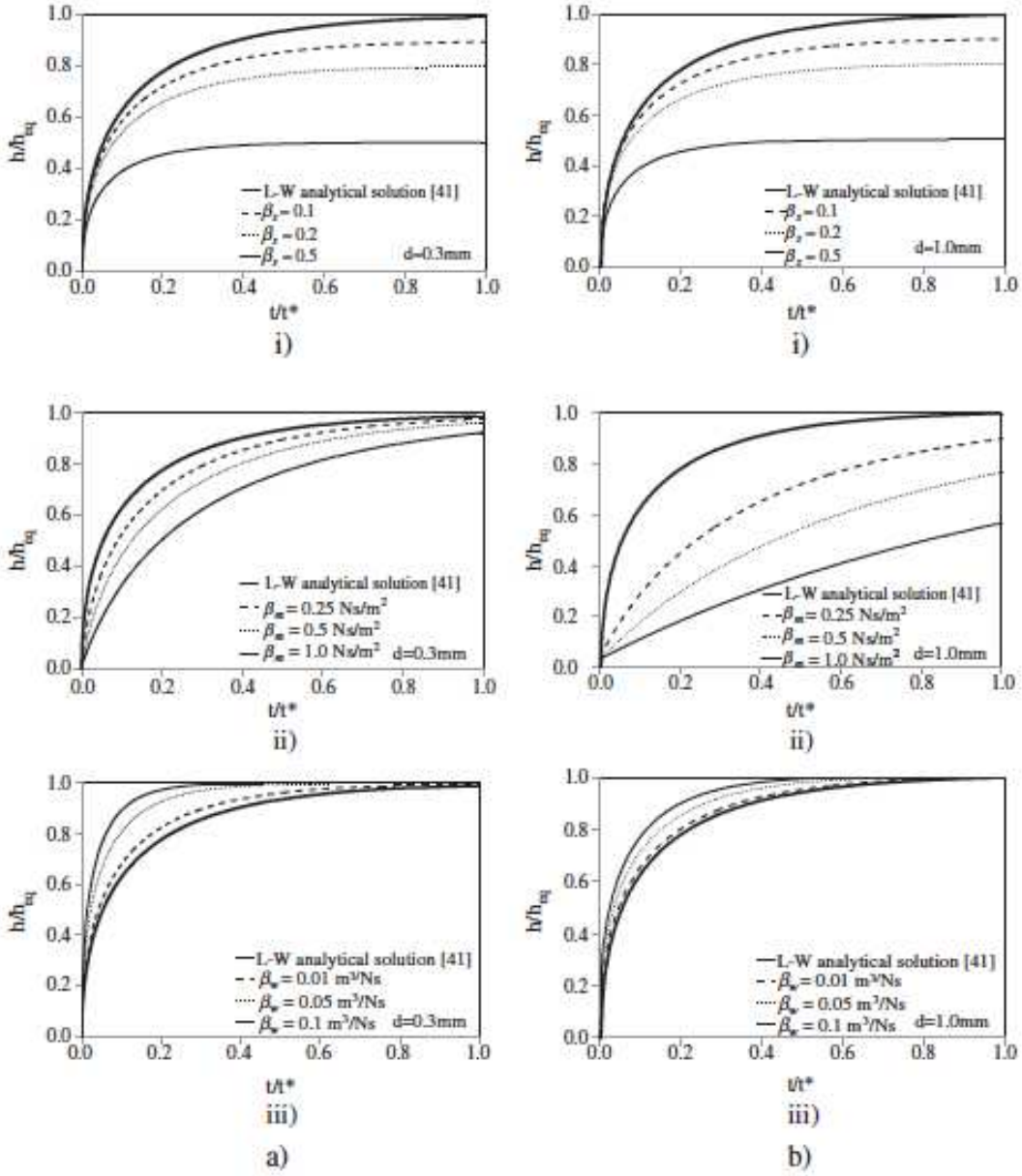

Figure 5-1. Effect of correction parameters i) βs, ii) βm and iii) βw on the capillary rise response of a) water in a glass capillary of diameter 0.30 mm b) water in a glass capillary of diameter 1.0 mm. Figure reproduced from Gardner et al. (2012).

On obtaining the equilibrium rise height, the β_s correction parameter is adjusted in the numerical simulation until the experimental rise height is achieved. The correction parameters β_m and β_w are then modified until the shape of the experimental capillary rise response is reproduced.

5.2 Analysis of results and discussion

The most representative and feasible experimental data have been used in order to compare the experimental results with the numerical solution. By acting in this way, the experimental data errors have been minimized, and consequently we avoid that the adjusted correction parameters may be covering up mistakes.

The resulting correction parameters are given in the figures 5-2 to 5-4 and summarized in the table 5-2.

Figure 5-2 displays the experimental and numerical results for a crack aperture of 0,2 mm in 7 and 365-day-old specimens in order to compare the different correction parameters between the young and the old specimens.

The graph shows that the difference between the experimental and numerical response is quite small in terms of capillary response time and also, equilibrium rise height. The correction parameters chosen try to be valid for both, C30 and C50 concrete strength.

Later, in figures 5-3 and 5-4 are showed a 365-day-old and 7-day-old experimental and numerical comparison respectively. The values of the correction parameters are similar to which reported in figure 5-2 and proves the repeatability of the results.

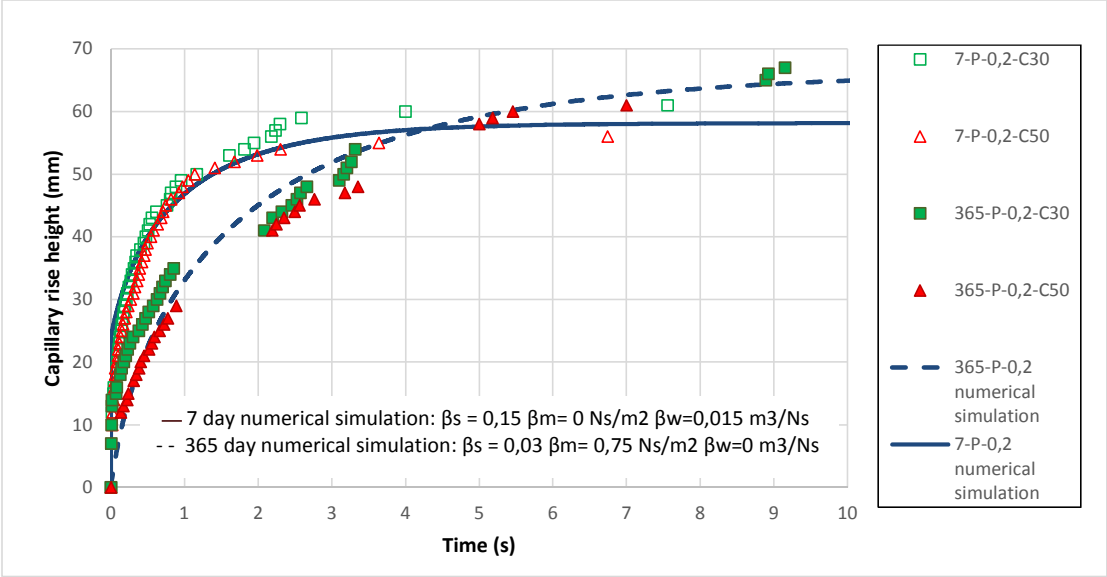

Figure 5-2. Comparison of experimental data to amended Lucas-Washburn equation for a planar crack of 0,2 mm in 7 and 365-day-old specimens

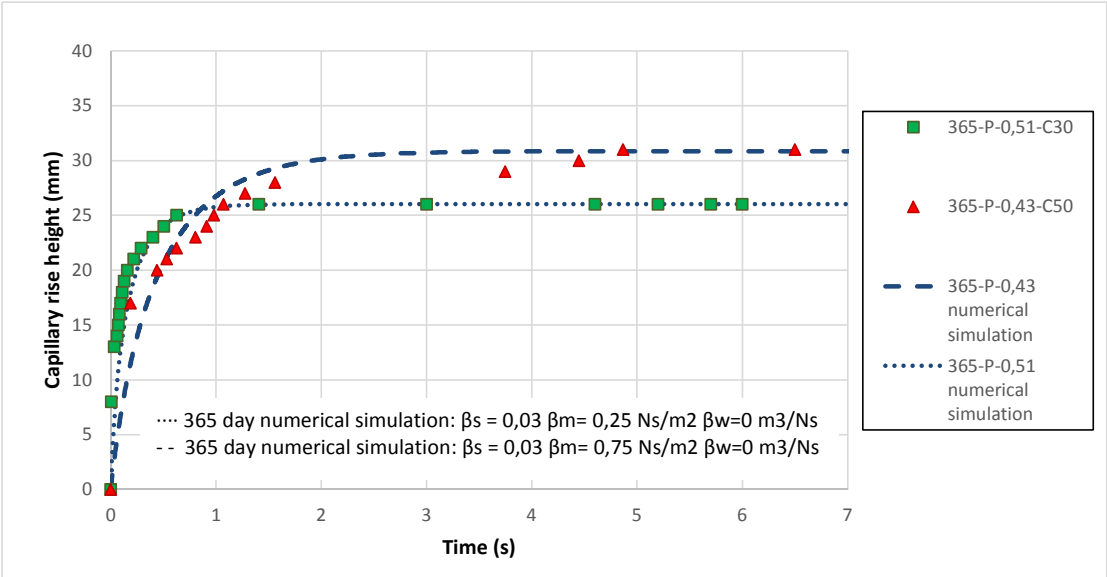

Figure 5-3. Comparison of experimental data to amended Lucas-Washburn equation for planar cracks of 0,43 and 0,51 mm in 365-day-old specimens

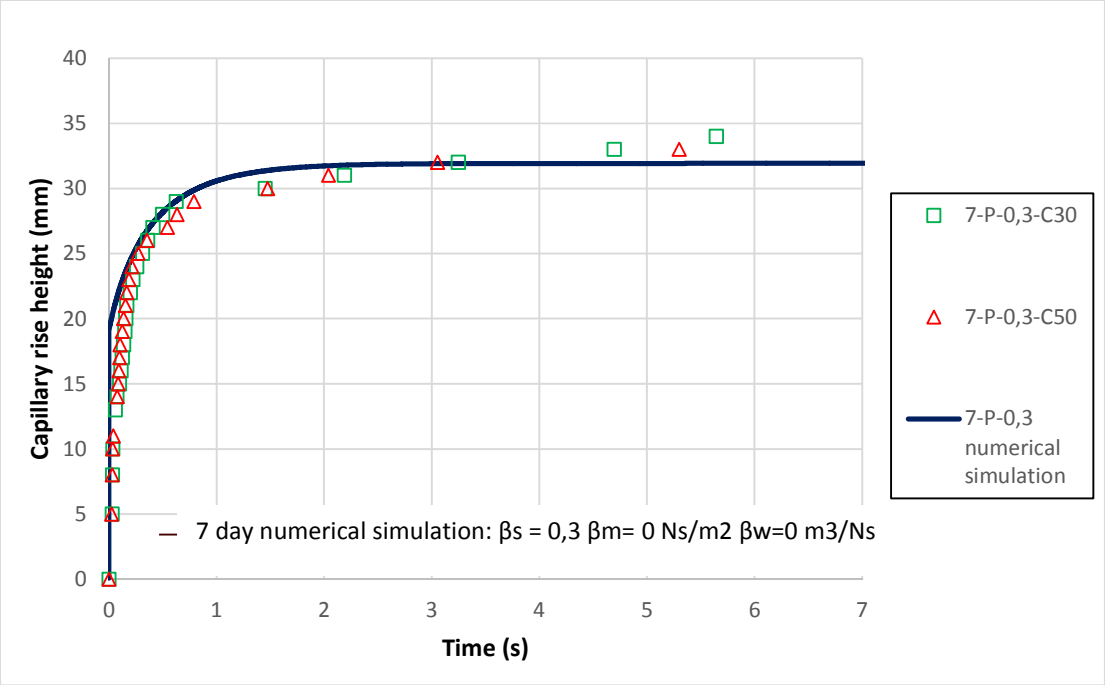

Figure 5-4. Comparison of experimental data to amended Lucas-Washburn equation for a planar crack of 0,3 mm in 7-day-old specimens

When considering the agreement between the theoretical and the experimental data it is apparent that a reasonably good agreement is achieved at crack apertures 0,2 mm and greater. This gives confidence in not only the experimental procedures used but also in the surface tension, contact angle and density values assumed in the theoretical solution.

It is evident that the correction parameters suggested in the figures 5-2 to 5-4 are consistent which the values collected from the previous studies in the Table 5-1.

The figure 5-2 shows that β_s decreases from 0,15 for the 7 day old specimen to 0,03 for the 365 day specimen. This observed reduction in the stick slip parameter with concrete age is attributed to changes in the mortar microstructure due to continued hydration, with the surface to which the adhesive adheres gradually becoming drier and denser as hydration proceeds. In the case shown in the 5-4 the value in the young element is even bigger (0,3).

On the other hand, It can also be observed that β_m assumes the value of 0,75 Ns/m^2 in the majority of the older specimens, the value of 0,25 Ns/m^2 in the 0,51 mm C30 crack aperture and 0 Ns/m^2 in the younger. This goes against what was commented in the chapter 2. Literature reviews, this correction parameter should be constant for any particular combination of material and fluid considered. The variation observed here is produced by the heterogeneous nature of the concrete macro structure at different ages and between specimens.

Finally, the β_w correction factor is 0 m^3/Ns in the majority of the cases, indicating no significant effect of wall slip on the capillary rise response of water in planar cracks in a cementitious material, with the exception of the 7-day-old in 0,2 mm crack aperture specimens, where it has a value of 0,015 m^3/Ns, which may be attributed to a boundary effect.

Crack width (mm)	**Specimen age**	**Concrete strenght**	**B_s (-)**	**B_m (Ns/m^2)**	**β_w (m^3/Ns)**
0,2	7 days	C30	0,15	0	0,015
0,2	7 days	C50	0,15	0	0,015
0,2	365 days	C30	0,03	0,75	0
0,2	365 days	C50	0,03	0,75	0
0,3	7 days	C30	0,3	0	0
0,3	7 days	C50	0,3	0	0
0,43	365 days	C50	0,03	0,25	0
0,51	365 days	C30	0,03	0,75	0

Table 5-2. Correction parameters for the simulation of experimental data

6 CONCLUSIONS

Below are listed the key conclusions from the experimental work and numerical simulation and how they can be applied to self-healing mechanisms in cementitious materials.

- As it was known, crack aperture affects the final rise height, with higher rise heights observed from smaller crack apertures as predicted by theory. This results have now been confirmed in concrete material.
- It has not been found a clear relation between the capillary rise response and the concrete strength. It would be necessary further measurements in order to get a better knowledge of this effect.
- Comparisons between old and young mortar specimens prove that the age of the specimen had an effect on the rate of capillary rise, being faster in young specimens and producing a retardation in matures. This may be attributed to the effect of the time dependent development of the mortar microstructure wall surface on the dynamic resistive forces acting during capillary rise.
- The relationship between the final capillary rise height measured for natural cracks and the final capillary rise height predicted for an equivalent planar crack has been adjusted in the upper part of the function (discrete crack bigger than 0.5mm), updating the parameters of the proposed Planar Equivalence Function and confirming the threshold value of the crack aperture 2 mm above which the capillary rise response for the planar and the natural crack is the same. Therefore, in future fluid flow could be determined for all healing agents with natural cracks based on planar experiments.
- At crack apertures greater or equal than 0,2 mm there is good agreement between the capillary flow response of the experimental data and the numerical solution based into the amended Lucas-Washburn equation.
- The correction factors in the amended Lucas-Washburn equation were adjusted in the numerical simulation until the experimental capillary rise height response was achieved. The correction parameter for stick–slip (β_s) decreases from the youngers specimens to the olders This is attributed to changes in the mortar microstructure due to continued

hydration, with the surface to which the adhesive adheres gradually becoming drier and denser as hydration proceeds. The correction parameter for frictional dissipation at the meniscus wall (β_m) reflects the heterogeneous surface roughness of the different concrete in the different ages. Finally, the correction parameter incorporating the slip between the fluid and solid wall (β_w) was 0 m^3/Ns in the majority of the cases which suggests that there is no significant influence of wall slip on the capillary rise response in these cases.

Comparisons between the experimental work and numerical solution show that the numerical solution is reliable to determine the flow theory for water. In the further works, the same experimental procedures should be conducted with healing agents to analyses the effect of the viscosity and the curing of the adhesive.

REFERENCES

Blake T.D. 1993. In: J.C. Berg Ed. *Wettability*. Marcel Dekker, New York,pp. 251-309

Bosanquet, C.H. 1923. On the flow of liquids into capillary tubes, *Philosophical Magazine* Series 6 Volume 45, pp. 525–531.

Carmeliet, J.,Delerue, J.-F., Vandersteen, K. and Roels, S. 2004. Three-dimensional liquid transport in concrete cracks. *International Journal for Numerical and Analytical Methods in Geomechanics* 28, pp. 671-687.

Chow T. 1998. Wetting of rough surfaces. *Journal of Physics: Condensed Matter* 10(27), pp. 445-451.

De Sitter, W.R. 1984. Costs for Service Life Optimization: The 'Law of Fives'", *Durability of Concrete Structures, Workshop Report*, Ed. Steen Rostam, Copenhagen, pp. 131- 134.

de Rooij, M., Van Tittelboom, K., De Belie, N. and Schlangen, E. 2013. *Self-Healing Phenomena in Cement-Based Materials*. State-of-the-Art Report of RILEM Technical Committee 221-SHC: Springer.

Delker, T., Pengra D. B. and Wong P.-Z. 1996. Interface Pinning and the Dynamics of Capillary Rise in Porous Media. *Physical review letters* 76(16), pp. 2902-2905.

Dry, C.1994.Matrix cracking repair and filling using active and passive modes for smart timed release of chemicals from fibers into cement matrices. *Smart Materials and Structures* 3(2), pp. 118-123.

Erickson, D., Li, D. and Park C. B. 2002. Numerical Simulations of Capillary-Driven Flows in Nonuniform Cross-Sectional Capillaries. *Journal of Colloid and Interface Science* 250, pp 422-430.

EUROCONSTRUCT, VTT, Buildecon cited in CEMBUREAU. The European Cement Association. Key facts and figures. Available at: http://bit.ly/R6g9ny [Last time accessed: 12/04/2014].

Eurostat. 2006. Cement and concrete production statistics - NACE Rev. 1.1. Available at: http://bit.ly/1rVfSRr [Last time accessed: 12/04/2014]

Fédération internationale du béton (fib). 2013. *Model Code for Concrete Structures 2010*. Lausanne.

Fenner, R., Ainger, C., Cruickshank, H. and Guthrie, P. 2006. Widening engineering horizons: addressing the complexity of sustainable development, *Proceedings of the Institution of Civil Engineers. Engineering Sustainability* 159, pp. 145-154.

Fries, N. and Dreyer, M. 2008. The transition from inertial to viscous flow in capillary rise. *Journal of Colloid and Interface Science* 327(1), pp. 125-128.

García A. Self-healing of open cracks in asphalt mastic. 2012. *Fuel* 93 pp. 264-272.

Gardner, D., Jefferson, A., Hoffman, A. and Lark, R. 2014. Simulation of the capillary flow of an autonomic healing agent in discrete cracks in cementitious materials. *Cement and Concrete Research* 58, pp. 35-44.

Gardner, D., Herbert, D., Jayaprakash, M. and Jefferson, A. 2013. Autonomic self-healing concrete: the capillary flow of cyanoacrylate in discrete cracks. *3rd Cement and Concrete Science Conference*. Portsmouth, UK, 2 - 3 September 2013.

Gardner, D., Jefferson, A., and Hoffman, A. 2012. Investigation of capillary flow in discrete cracks in cementitious materials. *Cement and Concrete Research* 42, pp. 972-981.

Gardner, D., Hoffman, A. and Jefferson, A. 2011. Capillary flow of healing agents in discrete cracks in cementitious materials. *3rd International Conference on Self-Healing Materials*. Bath, UK. 27-29 June 2011.

Hall, C.1989. Water sorptivity of mortars and concretes: a review. *Magazine of Concrete Research* 41(147), pp. 51-61.

Hamraoui, K., Thuresson, T., Nylander,V. and Yaminsky. 2000. Can a dynamic contact angle be understood in terms of a friction coefficient? *Journal of Colloid and Interface Science* 226, pp 199-204.

Hamraoui, A. and Nylander, T. 2002. Analytical Approach for the Lucas-Washburn Equation. Journal of Colloid and Interface Science, 250(2), pp. 415-421.

Hanzic, L. and Ilic, R. 2003. Relationship between liquid sorptivity and capillarity in concrete, *Cement and Concrete Research* 33 (9) pp. 1385-1388.

Hanzic, L., Kosec, L. and Anzel, I. 2010. Capillary absorption in concrete and the Lucas-Washburn equation. *Cement and Concrete Composites*, 32(1), pp. 84-91.

Hoffman, A. 2012. An Investigation into Flow Properties of Self-Healing Agents in Damaged Zones of Cementitious Materials. MPhil Thesis, Cardiff University.

Ichikawa, N., Hosokawa, K. and Maeda R. 2004. Interface motion of capillary-driven

flow in rectangular microchannel *Journal of Colloid and Interface Science* Volume 280, pp. 155–164.

IMF World Economic Outlook 2013, April 2013 cited in CEMBUREAU. The European Cement Association. Key facts and figures. Available at: http://bit.ly/R6g9ny [Last time accessed: 12/04/2014].

Jong, W.R., Kuoa, T.H. Ho, S.W., Chiua, H.H. and Peng S.H. 2007. Flows in rectangular microchannels driven by capillary force and gravity. *International Communications in Heat and Mass Transfer* Volume 34, pp. 186-196.

Joseph, C., Gardner, D., Jefferson, A.D., Isaacs B. and Lark, R. 2010a. Self-healing cementitious materials: a review of recent work. *Proceedings of the Institution of Civil Engineers. Construction Materials* 164, pp. 29-41.

Joseph, C., Jefferson, A.D., Isaacs, B., Lark, R. and Gardner, D.2010b. Experimental investigation of adhesive-based self-healing of cementitious materials. *Magazine of Concrete Research* 62(11), pp. 831–843.

Lago, M. and Araujo, M. 2001. Capillary rise in porous media, *Journal of Colloid and Interface Science* 234(1), pp. 35-43.

Lark, B. 2013. Materials for Life (M4L): Biomimetic multi-scale damage immunity for construction materials. In: EPSRC Network. Future Infrastructure Forum. University of Cambridge.

Lerner K.L. and Lerner B.W. 2004. *The GALE Encyclopedia of Science*. Thomson.

Li, V.C., Lim, Y.M. and Chan, Y.-W. 1998. Feasibility study of a passive smart self-healing cementitious composite. *Composites Part B: Engineering* 29(6), pp. 819-827.

Liou, W., Peng Y. and Parker, P.2009.Analytical modeling of capillary flow in tubes of nonuniform cross section. *Journal of Colloid and Interface Science* 333, pp. 389-399.

Lockington, D.A. and Parlange, J-Y. 2004. A new equation for macroscopic description of capillary rise in porous media, *Journal of Colloid and Interface Science* 278(2), pp. 404-409.

Martic, J.Coninck, and T.D.Blake. 2003, Influence of the dynamic contact angle on the characterization of porous media, *Journal of Colloid and Interface Science* 263 pp. 213–216.

Martys, N. S. and Ferraris, C. F. 1997. Capillary transport in mortars and concrete. *Cement and Concrete Research*, 27(5), pp. 747-760.

Mihashi, H., Kaneko, Y. and Nishiwaki, T., Otsuka, K. 2000. Fundamental study on development of intelligent concrete characterized by self-healing capability for strength. *Transactions of the Japan Concrete Institute* 22, pp. 441-450

Mooney, 1931. Explicit formulations for slip and fluidity, *Journal of Rheology 2*, pp. 210-222.

Murphy J.R. and Thomson N.R.1993. Two-Phase Flow in a Variable Aperture Fracture. *Water resources research*, 29 (10), pp. 3453-3476.

NACE Internacional, 2002. *Corrosion cost and preventive strategies in the United States*.

Neville,A.M. Properties of Concrete.2011.5th Edition. Pearson Education Ltd,Essex.

Quéré, D.1997. Inertial capillarity. *Europhysics Letters* 39(5) pp. 533–538.

Roels, S.,Vandersteen, K. and Carmeliet, J. 2003.Measuring and simulating moisture uptake in a fractured porous medium.*Advances in Water Resources*,26(3)pp.237-246

Schäffer, E. and Wong P. 2000. Contact line dynamics near the pinning threshold: A capillary rise and fall experiment. *Physical Review Letters* 61(5), pp. 5257-5277.

Schäffer, E. and Wong P. 1998. Dynamics of contact line pinning in capillary rise and fall. *Physical Review Letters* 80(14), pp. 3069-3072.

Shikhmurzaev Y. D. and Sprittles J. E. 2012. On the anomalous dynamics of capillary rise in porous media. arXiv:1206.6221.

Siebold, M. Nardin, J. Schultz, A. Walliser and M. Oppliger. 2000. Effect of dynamic contact angle on capillary rise phenomena. *Colloids and Surfaces*. A: Physicochemical and Engineering Aspects 161, pp. 81-87.

Söderqvist M. 2003. *Generic technical handbook for a predictive life cycle management system of concrete structures (LMS).* EU GROWTH Lifecon, Life Cycle Management of Concrete Infrastructures for Improved Sustainability, Deliverable D5.2. Available at: http://lifecon.vtt.fi/d11.pdf [Last time accessed: 12/04/2014].

Stalder, A.F., Kulik, G., Sage, D., Barbieri, L. and Hoffmann, P. 2006. A Snake-Based Approach to Accurate Determination of Both Contact Points and Contact Angles. *Colloids and Surfaces A: Physicochemical and Engineering Aspects*, 286(1-3) pp. 92-103.

Young W.-B. 2004. Analysis of capillary flows in non-uniform cross-sectional capillaries, *Colloids and Surfaces A: Physicochemical and Engineering Aspects 234*,

pp 123-128.

Wang J.S.Y. and Narasimhan T.N. 1985. Hydrologic mechanisms governing fluid flow in a partially saturated fractured porous medium. *Water resources research*, 21(12), pp. 1861-1874.

Washburn, E. W. 1921. The Dynamics of Capillary Flow. *Physical Review* 17(3), pp. 273-283.

White, S.R., Sottos, N.R., Geubelle, P.H., Moore, J.S., Kessler, M.R., Sriram, S.R., Brown, E.N. and Viswanathan, S. 2001. Autonomic healing of polymer composites. *Nature* 409, pp. 794-797.

Zimmerman W., Chen D. and Cook N. 1992. The effect of contact area on the permeability of fractures, *Journal of Hydrology 139*, pp. 79-96.

Zhmud, B. V., Tiberg. F. and Hallstensson K. 2000. Dynamics of Capillary Rise. *Journal of Colloid and Interface Science* 228, pp. 263-269.

APPENDIX A

Concrete mixes

Cement – OPC (Ordinary Porland Concrete)
Coarse aggregate - 10mm
Fine aggregate – 0 to 4 mm concreting sand

Strength	Mix proportions by mass			
	Cement	Fine aggregate	Coarse aggregate	Water
Weak C20-25	1,0	1,94	2,42	0,6
Medium C30-35	1,0	1,94	2,42	0,5
Strong C50-55	1,0	1,94	2,42	0,4

The table below is calculated assuming a concrete density of 2400kg/m^3

Strength	Mix proportions kg per m^3 of concrete			
	Cement	Fine aggregate	Coarse aggregate	Water
Weak C20-25	402,8	781,2	974,5	241,6
Medium C30-35	409,6	794,5	991,1	204,8
Strong C50-55	416,7	808,3	1008,3	166,7

C20-25

- Is a watery mix
- Not homogenous in nature
- Presence of voids is more

C30-35

- Appropriate Workability
- Homogenous mix
- Presence of voids is minimum

C50-55

- Less Workable
- Voids are minimum

APPENDIX B

Test results for cubes
C20 strength mix with 0,6 W/C ratio
0,2 & 0,3 apertures

Sample no.	Peak load, kN	Comp strength, N/mm^2	Length, mm	Width, mm	Height, mm	Mass, kg
1	225,1	22,26	100,20	100,10	100,90	2,410
2	231,0	22,60	100,80	100,50	101,40	2,400
3	234,2	23,05	100,90	100,20	100,70	2,390
Mean	230,1	**22,64**				
St dev		0,32				
COV, %		**1,42**				

0,1 aperture

Sample no.	Peak load, kN	Comp strength, N/mm^2	Length, mm	Width, mm	Height, mm	Mass, kg
1	222,1	22,06	100,20	97,15	100,50	2,318
2	209,0	20,84	100,00	100,00	100,30	2,378
3	212,2	20,93	100,20	100,25	101,20	2,402
Mean	214,4	**21,27**				
St dev		0,55				
COV, %		**2,61**				

Test results for cubes
C30 strength mix with 0,5 W/C ratio
0,2 & 0,3 apertures

Sample no.	Peak load, kN	Comp strength, N/mm^2	Length, mm	Width, mm	Height, mm	Mass, kg
1	372,2	36,74	100,40	100,10	100,90	2,430
2	373,1	36,94	100,20	100,20	100,80	2,440
3	379,3	37,48	100,50	100,25	100,70	2,460
Mean	374,9	**37,05**				
St dev		0,31				
COV, %		**0,84**				

0,1 aperture

Sample no.	Peak load, kN	Comp strength, N/mm^2	Length, mm	Width, mm	Height, mm	Mass, kg
1	399,1	39,69	100,00	100,35	100,55	2,464
2	395,1	39,49	99,90	100,25	100,15	2,431
3	409,0	40,86	100,00	99,90	100,10	2,434
Mean	401,1	**40,01**				
St dev		0,60				
COV, %		**1,51**				

Test results for cubes
C50 strength mix with 0,5 W/C ratio
0,2 & 0,3 apertures

Sample no,	Peak load, kN	Comp strength, N/mm^2	Length, mm	Width, mm	Height, mm	Mass, kg
1	375,4	37,13	100,20	100,10	100,90	2,465
2	387,1	37,73	100,40	100,30	102,20	2,470
3	397,5	39,05	100,20	100,30	101,60	2,480
Mean	386,7	**37,97**				
St dev		0,80				
COV, %		**2,11**				

0,1 aperture

Sample no,	Peak load, kN	Comp strength, N/mm^2	Length, mm	Width, mm	Height, mm	Mass, kg
1	593,0	58,08	100,50	99,90	101,60	2,490
2	602,0	59,14	100,00	99,95	101,80	2,490
3	608,0	59,76	99,75	100,40	102,00	2,501
Mean	601,0	**58,99**				
St dev		0,69				
COV, %		**1,18**				

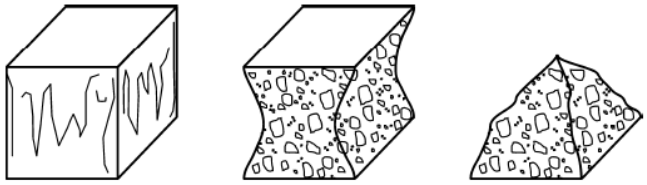

Explosive failure

NOTE All four exposed faces are cracked approximately equally, generally with little damage to faces in contact with the platens.

Figure 1 – Satisfactory failures of cube specimens

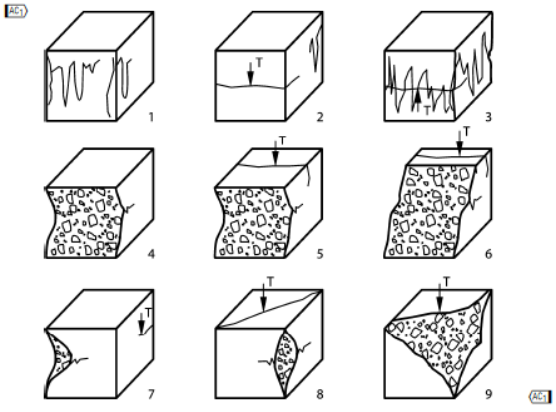

NOTE T = tensile crack

Figure 2 – Some unsatisfactory failures of cube specimens

1) Acceptable and 2) un-acceptable cube failure mechanisms for cube crushing tests.
Figure reproduced from BS EN 1230-3:2009.

APPENDIX C

Numeration of planar specimens

Concrete Strength	Crack aperture (mm)	Specimen numbers	Manufacture/ mix date	Observations
C20	0,1	1a 1b	03/04/13	lost
	0,2	1a 1b	25/02/13	
	0,3	2a 2b	25/02/13	
C30	0,1	2a 2b	08/04/13	lost
	0,2	2a 2b	18/02/13	
	0,3	2a 2b	18/02/13	
C50	0,1	2a 2b	10/04/13	
	0,2	4a 4b	27/02/13	
	0,3	3a 3b	27/02/13	

WP4 - concrete 0,004 sec per frame @250fps
Speciemen P-0.1-C20-UNSAT
Date manufactured 03/04/2013
Date tested 11/04/2013
Machined face

Height (mm)	Test 1 P-0.1-C20-UNSAT-1		Test 2 P-0.1-C20-UNSAT-2		Test 3 P-0.1-C20-UNSAT-3		Test 4 P-0.1-C20-UNSAT-4	
	Image no	time (s)	Image no	time (s)	Image no	time (s)	Image no	time (s)
0	100	0	13	0	15	0	4	0
1								
2								
3	103	0,012			18	0,012	5	0,004
4	104	0,016					7	0,012
5	105	0,02	14	0,004	19	0,016	9	0,02
6	106	0,024	17	0,016				
7	108	0,032			23	0,032		
8	109	0,036			24	0,036	10	0,024
9	111	0,044						
10			19	0,024			12	0,032
11			20	0,028			14	0,04
12	117	0,068	22	0,036	28	0,052	20	0,064
13	120	0,08	27	0,056	31	0,064	22	0,072
14	122	0,088	29	0,064	32	0,068	26	0,088
15	124	0,096	32	0,076	34	0,076	28	0,096
16	126	0,104	36	0,092	38	0,092	30	0,104
17	129	0,116	40	0,108	42	0,108		
18	132	0,128	43	0,12	43	0,112		
19	139	0,156	44	0,124			46	0,168
20	148	0,192			69	0,216	56	0,208
21	154	0,216	69	0,224	77	0,248	72	0,272
22	161	0,244	78	0,26	89	0,296	86	0,328
23	169	0,276	91	0,312	102	0,348	93	0,356
24	177	0,308	100	0,348	113	0,392	100	0,384
25	187	0,348	110	0,388	125	0,44	118	0,456
26	194	0,376	133	0,48	139	0,496	127	0,492
27	217	0,468	145	0,528	163	0,592	155	0,604
28	223	0,492	161	0,592	191	0,704	175	0,684
29	233	0,532	179	0,664	216	0,804	193	0,756
30	272	0,688	204	0,764	239	0,896	221	0,868
31	285	0,74	221	0,832	263	0,992	250	0,984
32	299	0,796	244	0,924	285	1,08	283	1,116
33	312	0,848	263	1	306	1,164	306	1,208
34	367	1,068	342	1,316	338	1,292	346	1,368
35	378	1,112	386	1,492	354	1,356	350	1,384
36	384	1,136	402	1,556	370	1,42	374	1,48
37	390	1,16	408	1,58	381	1,464	389	1,54
38	451	1,404	534	2,084	491	1,904	466	1,848
39	474	1,496	605	2,368	544	2,116	591	2,348
40	526	1,704	635	2,488	560	2,18	699	2,78

41	548	1,792	669	2,624	589	2,296	722	2,872
42	558	1,832	712	2,796	617	2,408	763	3,036
43	582	1,928	785	3,088	642	2,508	789	3,14
44	873	3,092	1019	4,024	851	3,344	920	3,664
45	1078	3,912	1169	4,624	1083	4,272	2292	9,152
46	1097	3,988	1191	4,712	1103	4,352	2309	9,22
47	1139	4,156	1266	5,012	1158	4,572	2353	9,396
48	1276	4,704	1398	5,54	1299	5,136	2470	9,864
49	1312	4,848	1597	6,336	1390	5,5	3076	12,288
50	1728	6,512	1623	6,44	1668	6,612	3137	12,532
51	4049	15,796	2081	8,272	2347	9,328	3679	14,7
52	4241	16,564	3070	12,228	2485	9,88	6544	26,16
53	4449	17,396	3185	12,688	2529	10,056	10970	43,864
54	4555	17,82	4444	17,724	2564	10,196	12373	49,476
55	4620	18,08	9640	38,508	2624	10,436	12438	49,736
56	5066	19,864	12963	51,8	3002	11,948	15251	60,988
57	7346	28,984			12174	48,636	15286	61,128
58					12447	49,728		
59								
60								
61								
62				220				
63								
64								
65								
66								
67								
68								
69								
70								
71								
72								

WP4 - concrete 0,004 sec per frame @250fps
Speciemen P-0.2-C20-UNSAT
Date manufactured 25/02/2013
Date tested 05/03/2013

Height (mm)	Test 1 P-0.2-C20-UNSAT-1		Test 2 P-0.2-C20-UNSAT-2		Test 3 P-0.2-C20-UNSAT-3	
	Image no	time (s)	Image no	time (s)	Image no	time (s)
0	1	0	503	0	497	0
1						
2	3	0,008				
3	5	0,016				
4	6	0,02				
5			508	0,02		
6			509	0,024	502	0,02
7					503	0,024
8	7	0,024	510	0,028	504	0,028
9	8	0,028	511	0,032	506	0,036
10	9	0,032		-2,012		
11	14	0,052	512			
12	16	0,06	513	0,04		
13	18	0,068	514	0,044	507	0,04
14	19	0,072	515	0,048	510	0,052
15			517	0,056	514	0,068
16			518	0,06	517	0,08
17	35	0,136	519	0,064	519	0,088
18	41	0,16	523	0,08	521	0,096
19	48	0,188	525	0,088	525	0,112
20	52	0,204	527	0,096	528	0,124
21	58	0,228	530	0,108	532	0,14
22	62	0,244	533	0,12	537	0,16
23	137	0,544	537	0,136	542	0,18
24	150	0,596	539	0,144	546	0,196
25	178	0,708	543	0,16	548	0,204
26	237	0,944	546	0,172	552	0,22
27	259	1,032	552	0,196	556	0,236
28	281	1,12	555	0,208	559	0,248
29	299	1,192			562	0,26
30	314	1,252	567	0,256	573	0,304
31	320	1,276	573	0,28	577	0,32
32	331	1,32	581	0,312	581	0,336
33	345	1,376	590	0,348	587	0,36
34	419	1,672	597	0,376	600	0,412
35	448	1,788	622	0,476	629	0,528
36	457	1,824	631	0,512	655	0,632
37	468	1,868	640	0,548	660	0,652
38	487	1,944	655	0,608	668	0,684
39	520	2,076	668	0,66	677	0,72
40	551	2,2	675	0,688	700	0,812
41	714	2,852	692	0,756	727	0,92
42	821	3,28	725	0,888	735	0,952
43	1000	3,996	741	0,952	740	0,972

44	1209	4,832	862	1,436	749	1,008
45	1234	4,932			764	1,068
46	1261	5,04			781	1,136
47	1283	5,128			792	1,18
48	1350	5,396			806	1,236
49	1376	5,5			836	1,356
50	1420	5,676			861	1,456
51	1517	6,064			906	1,636
52	1582	6,324			946	1,796
53	1820	7,276			1026	2,116
54	2068	8,268			1067	2,28
55	2312	9,244			1170	2,692
56	2355	9,416			1241	2,976
57					1254	3,028
58						
59						
60	5052	20,204				
61	5174	20,692			2680	8,732
62	5300	21,196			2733	8,944
63	5480	21,916			2757	9,04
64	5517	22,064			2826	9,316
65	5568	22,268			2870	9,492
66	5750	22,996			2929	9,728
67	6335	25,336			3498	12,004
68						
69						
70						
71						
72		35,1				26,2

WP4 - concrete 0,004 sec per frame @250fps
Speciemen P-0.3-C20-UNSAT
Date manufactured 25/02/2013
Date tested 05/03/2013

Height (mm)	Test 1 P-0.3-C20-UNSAT-1		Test 2 P-0.3-C20-UNSAT-2		Test 3 P-0.3-C20-UNSAT-3	
	Image no	time (s)	Image no	time (s)	Image no	time (s)
0	552	0	1	0	4	0
1						
2						
3						
4						
5	554	0,008		-0,004		
6					8	0,016
7					9	0,02
8			10	0,036		
9						
10			13	0,048	12	0,032
11	557	0,02	17	0,064	13	0,036
12	559	0,028				
13			21			
14	562	0,04		-0,004	18	0,056
15	564	0,048	32	0,124	19	0,06
16	565	0,052	33	0,128	23	0,076
17	566	0,056	37	0,144	26	0,088
18	572	0,08	44	0,172	30	0,104
19	576	0,096	52	0,204	37	0,132
20	582	0,12	56	0,22	45	0,164
21	587	0,14	60	0,236	52	0,192
22	594	0,168	65	0,256	61	0,228
23	598	0,184	71	0,28	71	0,268
24	604	0,208	76	0,3	91	0,348
25	610	0,232	80	0,316	103	0,396
26	613	0,244	89	0,352	508	2,016
27	629	0,308	105	0,416	867	3,452
28	654	0,408	216	0,86	1019	4,06
29	753	0,804	243	0,968	1282	5,112
30	867	1,26	291	1,16	1613	6,436
31	921	1,476	354	1,412	2005	8,004
32	1029	1,908	373	1,488	9499	37,98
33	1145	2,372	406	1,62	10582	42,312
34	1190	2,552	516	2,06	11067	44,252
35	1215	2,652	1398	5,588		
36	1311	3,036	2211	8,84		
37	1361	3,236	2315	9,256		
38	1398	3,384	2441	9,76		
39	1435	3,532	2672	10,684		
40	1504	3,808	2878	11,508		
41	1861	5,236	4054	16,212		
42	2508	7,824	17772	71,084		
43	2615	8,252				

WP4 - concrete 0,004 sec per frame @250fps
Speciemen P-0.1-C30-UNSAT
Date manufactured 08/04/2013
Date tested 16/04/2013

Height (mm)	Test 1 P-0.1-C30-UNSAT-1		Test 2 P-0.1-C30-UNSAT-2		Test 3 P-0.1-C30-UNSAT-3	
	Image no	time (s)	Image no	time (s)	Image no	time (s)
0	40	0	46	0	50	0
1						
2						
3						
4						
5			49	0,012	53	0,012
6						
7			56	0,04		
8			57	0,044	54	0,016
9			58	0,048		
10						
11	41	0,004				
12	43	0,012			56	0,024
13	45	0,02	59	0,052	58	0,032
14	47	0,028	60	0,056	59	0,036
15	49	0,036	62	0,064	61	0,044
16	50	0,04	64	0,072	63	0,052
17	52	0,048			66	0,064
18			67	0,084	67	0,068
19			83	0,148		
20	58	0,072	91	0,18	85	0,14
21	74	0,136	98	0,208	93	0,172
22	79	0,156	107	0,244	102	0,208
23	85	0,18	113	0,268	113	0,252
24	92	0,208	124	0,312	123	0,292
25	97	0,228	136	0,36	131	0,324
26	105	0,26	154	0,432	148	0,392
27	116	0,304	168	0,488	158	0,432
28	129	0,356	190	0,576	166	0,464
29	143	0,412	209	0,652	175	0,5
30	156	0,464	226	0,72	191	0,564
31	165	0,5	255	0,836	215	0,66
32	177	0,548	273	0,908	237	0,748
33	197	0,628	297	1,004	257	0,828
34	219	0,716	333	1,148	285	0,94
35	240	0,8	347	1,204	312	1,048
36	263	0,892	368	1,288	339	1,156
37	293	1,012	396	1,4	372	1,288
38	324	1,136	416	1,48	409	1,436
39	356	1,264	460	1,656	437	1,548
40	387	1,388	512	1,864	472	1,688
41	454	1,656	531	1,94	530	1,92
42	482	1,768	566	2,08	562	2,048

43	507	1,868	588	2,168	580	2,12
44	561	2,084	628	2,328	620	2,28
45	591	2,204	657	2,444	649	2,396
46	615	2,3	691	2,58	671	2,484
47	682	2,568	741	2,78	726	2,704
48	720	2,72	786	2,96	772	2,888
49	782	2,968	866	3,28	852	3,208
50	955	3,66	984	3,752	940	3,56
51	997	3,828	1062	4,064	1038	3,952
52	1041	4,004	1117	4,284	1110	4,24
53	1066	4,104	1176	4,52	1157	4,428
54	1162	4,488	1235	4,756	1241	4,764
55	1204	4,656	1300	5,016	1290	4,96
56			1424	5,512	1382	5,328
57			1485	5,756	1468	5,672
58					1541	5,964
59	1719	6,716			1584	6,136
60	1769	6,916	1688	6,568		
61	1892	7,408	1875	7,316	1798	6,992
62	1951	7,644	2086	8,16	2061	8,044
63	2179	8,556	2256	8,84	2391	9,364
64	2800	11,04	2337	9,164	2572	10,088
65	4187	16,588	2786	10,96	3112	12,248
66			2879	11,332	3208	12,632
67			2951	11,62	3373	13,292
68			3383	13,348	3814	15,056
69			3577	14,124	5151	20,404
70		180	5045	19,996	11336	45,144

WP4 - concrete 0,004 sec per frame @250fps
Speciemen P-0.2-C30-UNSAT
Date manufactured 18/02/2013
Date tested 26/02/2013

Height (mm)	Test 1 P-0.2-C30-UNSAT-1		Test 2 P-0.2-C30-UNSAT-2		Test 3 P-0.2-C30-UNSAT-3	
	Image no	time (s)	Image no	time (s)	Image no	time (s)
0	1	0	1	0	4	0
1						
2						
3						
4						
5					7	0,012
6						
7						
8					9	0,02
9						
10	3	0,008			10	0,024
11					12	0,032
12			5	0,016	13	0,036
13	5	0,016			19	0,06
14	6	0,02			21	0,068
15	7	0,024	10	0,036	22	0,072
16	9	0,032	11	0,04	24	0,08
17	10	0,036			26	0,088
18	12	0,044			27	0,092
19			21	0,08	28	0,096
20	13	0,048	23	0,088	33	0,116
21	18	0,068	25	0,096	35	0,124
22	21	0,08	27	0,104	38	0,136
23	25	0,096	29	0,112	41	0,148
24	30	0,116	31	0,12	46	0,168
25	34	0,132	36	0,14	52	0,192
26	38	0,148	38	0,148	56	0,208
27	42	0,164	42	0,164	66	0,248
28	47	0,184	45	0,176	71	0,268
29	51	0,2	49	0,192	78	0,296
30	55	0,216	54	0,212	95	0,364
31	59	0,232	56	0,22	112	0,432
32	66	0,26	62	0,244	118	0,456
33	72	0,284	68	0,268	134	0,52
34	80	0,316	73	0,288	141	0,548
35	86	0,34	79	0,312	148	0,576
36	97	0,384	84	0,332	164	0,64
37	103	0,408	88	0,348	188	0,736
38	111	0,44	101	0,4	224	0,88
39	126	0,5	113	0,448	255	1,004
40	139	0,552	120	0,476	307	1,212
41	151	0,6	127	0,504	331	1,308
42	164	0,652	132	0,524	399	1,58

43	261	1,04	140	0,556	730	2,904
44	338	1,348	155	0,616	1191	4,748
45	349	1,392	191	0,76	1472	5,872
46	358	1,428	202	0,804	1727	6,892
47	375	1,496	206	0,82	5303	21,196
48	1729	6,912	221	0,88	5798	23,176
49	1934	7,732	239	0,952	6348	25,376
50	2013	8,048	292	1,164	10536	42,128
51	2060	8,236			10629	42,5
52	2109	8,432			11032	44,112
53	2173	8,688	403	1,608	11071	44,268
54	2177	8,704	454	1,812	11085	44,324
55	2179	8,712	487	1,944	11210	44,824
56	2213	8,848	545	2,176	11264	45,04
57	2241	8,96	560	2,236	11405	45,604
58			575	2,296	11482	45,912
59			647	2,584	12097	48,372
60			1000	3,996		
61			1890	7,556		
62						
63	4247	16,984				
64	4287	17,144				
65	4296	17,18				
66	4314	17,252				
67	4447	17,784				
68	4467	17,864		58		
69	4578	18,308				
70						

Height (mm)	Test 1 P-0.3-C30-UNSAT-1		Test 2 P-0.3-C30-UNSAT-2		Test 3 P-0.3-C30-UNSAT-3	
	Image no	time (s)	Image no	time (s)	Image no	time (s)
0	2	0	1	0	4	0
1						
2					6	0,008
3					9	0,02
4					12	0,032
5	6	0,016	8	0,028	15	0,044
6	7	0,02			17	0,052
7	9	0,028			19	0,06
8	10	0,032	9	0,032	22	0,072
9	11	0,036			23	0,076
10			10	0,036	24	0,08
11					30	0,104
12					35	0,124
13	14	0,048	16	0,06	37	0,132
14	16	0,056	19	0,072		
15	19	0,068	25	0,096		
16	21	0,076	29	0,112	50	0,184
17	24	0,088	32	0,124	52	0,192
18	26	0,096	35	0,136	57	0,212
19	28	0,104	38	0,148	63	0,236
20	30	0,112	40	0,156	66	0,248
21	36	0,136	42	0,164	68	0,256
22	39	0,148	50	0,196	70	0,264
23	42	0,16	56	0,22	78	0,296
24	44	0,168	65	0,256	80	0,304
25	48	0,184	79	0,312	83	0,316
26	50	0,192	91	0,36	87	0,332
27	55	0,212	103	0,408	91	0,348
28	59	0,228	125	0,496	95	0,364
29	64	0,248	157	0,624	99	0,38
30	68	0,264	364	1,452	104	0,4
31	75	0,292	548	2,188	111	0,428
32	79	0,308	813	3,248	115	0,444
33	83	0,324	1175	4,696	120	0,464
34	88	0,344	1412	5,644	125	0,484
35	97	0,38	1859	7,432	133	0,516
36	112	0,44	2127	8,504	142	0,552
37	129	0,508	2230	8,916	155	0,604
38	146	0,576	2604	10,412	191	0,748
39	175	0,692	3424	13,692	217	0,852
40	192	0,76	5118	20,468	233	0,916
41	229	0,908	6092	24,364	275	1,084
42	251	0,996			286	1,128
43	283	1,124			314	1,24
44	322	1,28			404	1,6
45	420	1,672			614	2,44
46	427	1,7			1187	4,732
47	440	1,752			1224	4,88

48	472	1,88			1273	5,076
49	629	2,508			1343	5,356
50	6299	25,188			4842	19,352
51					8667	34,652
52					8787	35,132
53					8962	35,832
54						
55						
56						

WP4 - concrete 0,004 sec per frame @250fps
Speciemen P-0.1-C50-UNSAT
Date manufactured 10/04/2013
Date tested 18/04/2013

Height (mm)	Test 2 P-0.1-C50-UNSAT-2		Test 3 P-0.1-C50-UNSAT-3		Test 4 P-0.1-C50-UNSAT-4	
	Image no	time (s)	Image no	time (s)	Image no	time (s)
0	-433	0	-541	0	37	0
1						
2						
3			-540	0,004		
4	-432	0,004	-537	0,016		
5					38	0,004
6	-422	0,044	-523	0,072	39	0,008
7					40	0,012
8	-421	0,048				
9	-420	0,052	-514	0,108		
10	-418	0,06			49	0,048
11			-513	0,112	51	0,056
12			-512	0,116	52	0,06
13			-509	0,128	53	0,064
14	-417	0,064	-508	0,132	56	0,076
15	-415	0,072	-506	0,14	59	0,088
16	-413	0,08	-503	0,152	61	0,096
17	-410	0,092	-501	0,16	63	0,104
18	-408	0,1	-499	0,168	66	0,116
19	-405	0,112	-498	0,172	67	0,12
20	-401	0,128	-491	0,2	68	0,124
21	-397	0,144	-473	0,272	83	0,184
22	-391	0,168	-459	0,328	90	0,212
23	-386	0,188	-445	0,384	97	0,24
24	-376	0,228	-433	0,432	112	0,3
25	-369	0,256	-421	0,48	134	0,388
26	-361	0,288	-410	0,524	156	0,476
27	-351	0,328	-399	0,568	165	0,512
28	-338	0,38	-374	0,668	182	0,58
29	-326	0,428	-360	0,724	200	0,652
30	-316	0,468	-338	0,812	221	0,736
31	-303	0,52	-323	0,872	245	0,832
32	-290	0,572	-299	0,968	270	0,932
33	-266	0,668	-277	1,056	295	1,032
34	-245	0,752	-264	1,108	331	1,176
35	-234	0,796	-244	1,188	349	1,248
36	-225	0,832	-211	1,32	361	1,296
37	-202	0,924	-193	1,392	375	1,352
38	-185	0,992	-177	1,456	386	1,396
39	-102	1,324	-123	1,672	405	1,472
40	-69	1,456	-20	2,084	498	1,844
41	-31	1,608	13	2,216	542	2,02
42	20	1,812	33	2,296	622	2,34

43	49	1,928	77	2,472	642	2,42
44	82	2,06	107	2,592	691	2,616
45	185	2,472	212	3,012	831	3,176
46	209	2,568	272	3,252	966	3,716
47	231	2,656	298	3,356	990	3,812
48	289	2,888	347	3,552	1048	4,044
49	368	3,204	391	3,728	1157	4,48
50	408	3,364	423	3,856	1194	4,628
51	460	3,572	484	4,1	1233	4,784
52	500	3,732	501	4,168	1242	4,82
53	511	3,776	521	4,248	1255	4,872
54	529	3,848	542	4,332	1285	4,992
55	562	3,98	561	4,408	1307	5,08
56	621	4,216			1383	5,384
57	682	4,46			1447	5,64
58	710	4,572	1054	6,38		
59	733	4,664	1161	6,808		
60			2467	12,032		
61			2886	13,708	3834	15,188
62			4365	19,624	4049	16,048
63	4992	21,7	8559	36,4	5592	22,22
64	8053	33,944	13269	55,24	17729	70,768
65	11244	46,708				
66						
67						
68						
69						
70						

WP4 - concrete 0,004 sec per frame @250fps
Speciemen P-0.2-C50-UNSAT
Date manufactured 27/02/2013
Date tested 07/03/2013

Height (mm)	Test 1 P-0.2-C50-UNSAT-1		Test 2 P-0.2-C50-UNSAT-2		Test 3 P-0.2-C50-UNSAT-3	
	Image no	time (s)	Image no	time (s)	Image no	time (s)
0	3	0	1	0	10	0
1						
2						
3	4	0,004				
4					12	0,008
5	5	0,008			15	0,02
6	6	0,012				
7	7	0,016				
8					17	0,028
9						
10			6	0,02		
11						
12			7	0,024	20	0,04
13			9	0,032	21	0,044
14	11	0,032	11	0,04	22	0,048
15	12	0,036	12	0,044	23	0,052
16	13	0,04	13	0,048	26	0,064
17	14	0,044	14	0,052	27	0,068
18	15	0,048	15	0,056	28	0,072
19	27	0,096	16	0,06	32	0,088
20	29	0,104	21	0,08	41	0,124
21	33	0,12	25	0,096	44	0,136
22	38	0,14	26	0,1	48	0,152
23	43	0,16	30	0,116	53	0,172
24	48	0,18	35	0,136	60	0,2
25	56	0,212	38	0,148	65	0,22
26	64	0,244	42	0,164	72	0,248
27	76	0,292	47	0,184	80	0,28
28	85	0,328	54	0,212	86	0,304
29	98	0,38	60	0,236	96	0,344
30	121	0,472	68	0,268	109	0,396
31	150	0,588	77	0,304	122	0,448
32	202	0,796	83	0,328	134	0,496
33	308	1,22	90	0,356	162	0,608
34	1434	5,724	95	0,376		
35	1814	7,244	99	0,392		
36	6186	24,732	106	0,42	322	1,248
37	6738	26,94	114	0,452	431	1,684
38			118	0,468	541	2,124
39			125	0,496	602	2,368
40			137	0,544	646	2,544
41			146	0,58	708	2,792
42			160	0,636	837	3,308

43		168	171	0,68	1560	6,2
44			178	0,708	2355	9,38
45			187	0,744	2526	10,064
46			205	0,816	2725	10,86
47			231	0,92	2765	11,02
48			244	0,972	2808	11,192
49			264	1,052	2946	11,744
50			285	1,136	3067	12,228
51			353	1,408	3289	13,116
52			420	1,676	3746	14,944
53			497	1,984	5118	20,432
54			577	2,304		
55			911	3,64		
56			1686	6,74		
57						
58						
59						
60						
61						
62						
63						
64						
65						
66						
67						
68						
69						
70						

WP4 - concrete 0,004 sec per frame @250fps
Speciemen P-0.3-C50-UNSAT
Date manufactured 27/02/2013
Date tested 07/03/2013

Height (mm)	Test 1 P-0.3-C50-UNSAT-1		Test 2 P-0.3-C50-UNSAT-2		Test 3 P-0.3-C50-UNSAT-3	
	Image no	time (s)	Image no	time (s)	Image no	time (s)
0	11	0	5	0	1	0
1						
2						
3					7	0,024
4					8	0,028
5			11	0,024		
6					9	0,032
7	20	0,036				
8	21	0,04	12	0,028		
9	22	0,044				
10	23	0,048	13	0,032	11	0,04
11			15	0,04		
12						
13					26	0,1
14	25	0,056	24	0,076		
15	26	0,06	26	0,084	32	
16	32	0,084	28	0,092	38	0,148
17	34	0,092	29	0,096	41	0,16
18	36	0,1	31	0,104		
19	38	0,108	36	0,124	94	0,372
20	210	0,796	39	0,136	110	0,436
21	230	0,876	43	0,152	128	0,508
22	273	1,048	46	0,164	150	0,596
23	315	1,216	51	0,184	197	0,784
24	471	1,84	58	0,212	266	1,06
25	519	2,032	73	0,272	378	1,508
26	572	2,244	93	0,352	639	2,552
27	659	2,592	140	0,54	832	3,324
28	802	3,164	163	0,632	1168	4,668
29	933	3,688	202	0,788	1470	5,876
30	1114	4,412	374	1,476	1680	6,716
31	1369	5,432	515	2,04	1893	7,568
32	1722	6,844	768	3,052	2214	8,852
33	1954	7,772	1330	5,3	2431	9,72
34	2544	10,132			2954	11,812
35	4521	18,04			4033	16,128
36	4698	18,748			5645	22,576
37	6706	26,78				
38						180
39						
40						

Height (mm)	Test 1 20140314 P-0.2-C20-UNS-LONG		Test 2 20140317 P-0.2-C20-UNS-LONG		Test 3 20140320 P-0.2-C20-UNS-LONG	
	Image no	time (s)	Image no	time (s)	Image no	time (s)
0	184	0	296	0	325	0
1						
2						
3						
4						
5						
6						
7						
8						
9			297	0,004		
10						
11					327	0,008
12	423	0,956				
13	470	1,144	298	0,008		
14	491	1,228				
15	536	1,408	299	0,012		
16			300	0,016		
17					330	0,02
18			301	0,02	5018	18,772
19	1103	3,676			11215	43,56
20	1149	3,86			15056	58,924
21	1236	4,208	303	0,028	15901	62,304
22	1303	4,476			16235	63,64
23	1471	5,148	409	0,452	19591	77,064
24	1677	5,972	1229	3,732		
25	1720	6,144	6734	25,752		
26	1750	6,264	9653	37,428		
27	1786	6,408	11522	44,904		
28	1809	6,5				
29	1868	6,736				
30	1919	6,94				
31	1945	7,044				
32						
33						
34						
35						
36						
37						
38						
39						
40						
41						
42						
43						
44						
45						
46						
47						
48						

49						
50						
51						
52	3200	12,064				
53						
54						
55	3379	12,78				
56						
57	3471	13,148				
58						
59						
60						

Height (mm)	Test 1 20140318 P-0.3-C20-UNS-LONG		Test 2 20140320 P-0.3-C20-UNS-LONG		Test 3 20140321 P-0.3-C20-UNS-LONG	
	Image no	time (s)	Image no	time (s)	Image no	time (s)
0	337	0	177	0	257	0
1						
2						
3						
4						
5						
6						
7						
8						
9						
10						
11	340	0,012			259	0,008
12						
13	341	0,016			260	0,012
14			180	0,012		
15	342	0,02				
16						
17	475	0,552				
18	640	1,212	183	0,024		
19	857	2,08	896	2,876		
20	998	2,644	1086	3,636		
21	1587	5	4557	17,52	262	0,02
22	6089	23,008			7016	27,036
23	8193	31,424			9812	38,22
24	8731	33,576			13906	54,596
25						
26						
27						
28						
29						
30						
31						
32						
33						
34						
35						
36						
37						
38						
39						
40						
41						
42						
43						
44						

Height (mm)	Test 1	20140318	Test 2	20140321	Test 3	20140325
	P-0.2-C30-UNS-LONG		P-0.2-C30-UNS-LONG		P-0.2-C30-UNS-LONG	
	Image no	time (s)	Image no	time (s)	Image no	time (s)
0	179	0	122	0	117	0
1						
2						
3						
4						
5						
6						
7	180	0,004				
8						
9						
10	181	0,008			118	0,004
11			124	0,008		
12						
13	182	0,012				
14	183	0,016				
15	196	0,068				
16	199	0,08				
17						
18	211	0,128			120	0,012
19	215	0,144	126	0,016	967	3,4
20	223	0,176	776	2,616	1034	3,668
21	229	0,2	1008	3,544	1167	4,2
22	235	0,224	1145	4,092	1254	4,548
23	243	0,256	1248	4,504	1321	4,816
24	254	0,3	1310	4,752	1364	4,988
25	273	0,376	1383	5,044	1514	5,588
26	286	0,428	1453	5,324	1465	5,392
27	297	0,472	1478	5,424	1614	5,988
28	307	0,512	1502	5,52	1671	6,216
29	322	0,572	1523	5,604	1782	6,66
30	336	0,628	1591	5,876	1946	7,316
31	345	0,664	2086	7,856	5242	20,5
32	354	0,7	2094	7,888	5269	20,608
33	364	0,74	2104	7,928	5291	20,696
34	380	0,804	2113	7,964	5315	20,792
35	392	0,852			5323	20,824
36					5350	20,932
37					5505	21,552
38						
39						
40						
41	700	2,084				
42						
43	728	2,196	3175	12,212		
44	759	2,32	3413	13,164		
45	793	2,456	3578	13,824		
46	810	2,524	12751	50,516		

47	823	2,576				
48	844	2,66				
49	954	3,1				
50	969	3,16				
51	980	3,204				
52	995	3,264				
53						
54	1008	3,316				
55						
56						
57						
58						
59						
60						
61						
62						
63						
64						
65	2401	8,888				
66	2410	8,924				
67	2466	9,148				
68						
69						
70						

Height (mm)	Test 1	20140314	Test 2	20140319	Test 3	20140324
	P-0.51-C30-UNS-LONG		P-0.51-C30-UNS-LONG		P-0.51-C30-UNS-LONG	
	Image no	time (s)	Image no	time (s)	Image no	time (s)
0	178	0	178	0	277	0
1						
2						
3						
4						
5						
6						
7						
8	179	0,004				
9						
10					298	0,084
11					307	0,12
12					394	0,468
13	186	0,032	181	0,012	1024	2,988
14	193	0,06	286	0,432	1382	4,42
15	196	0,072	315	0,548	1715	5,752
16	198	0,08	330	0,608	1810	6,132
17	201	0,092	343	0,66		
18	205	0,108	742	2,256		
19	210	0,128				
20	218	0,16	819	2,564	3050	11,092
21	232	0,216	845	2,668	3265	11,952
22	250	0,288	947	3,076	3647	13,48
23	278	0,4	1011	3,332	4020	14,972
24	304	0,504	1075	3,588	4221	15,776
25	334	0,624	1122	3,776	4603	17,304
26	530	1,408	1229	4,204	5519	20,968
27			3120	11,768	7088	27,244
28					7963	30,744
29						
30						
31						
32						
33						
34						
35						
36						
37						
38						
39						
40						
41						
42						
43						
44						
45						

Height (mm)	Test 1 20140317 P-0.2-C50-UNS-LONG		Test 2 20140318 P-0.2-C50-UNS-LONG		Test 3 20140319 P-0.2-C50-UNS-LONG	
	Image no	time (s)	Image no	time (s)	Image no	time (s)
0	329	0	229	0	304	0
1						
2						
3						
4						
5						
6						
7			230	0,004		
8						
9			231	0,008		
10						
11			233	0,016		
12	363	0,136			306	0,008
13	372	0,172			663	1,436
14	384	0,22	1411	4,728	973	2,676
15	388	0,236	1436	4,828	1081	3,108
16			1463	4,936		
17	406	0,308	1504	5,1		
18	415	0,344	1561	5,328		
19	424	0,38	1625	5,584	1193	3,556
20	430	0,404	1682	5,812	1222	3,672
21	441	0,448	1720	5,964	1253	3,796
22	459	0,52	1797	6,272	1297	3,972
23	468	0,556	1924	6,78	1342	4,152
24	477	0,592	1997	7,072	1409	4,42
25	494	0,66	2150	7,684	1444	4,56
26	509	0,72	2754	10,1	1487	4,732
27	522	0,772	2835	10,424	1745	5,764
28			2866	10,548	2202	7,592
29	551	0,888	2923	10,776	4000	14,784
30			2941	10,848	4047	14,972
31			2952	10,892	4160	15,424
32			2963	10,936	4196	15,568
33					4234	15,72
34						
35						
36						
37						
38						
39						
40			11420	44,764		
41	877	2,192	12431	48,808		
42	890	2,244	12674	49,78		
43	917	2,352	13124	51,58		
44	953	2,496	13308	52,316		
45	969	2,56	13827	54,392		
46	1020	2,764				
47	1123	3,176				

48	1167	3,352				
49	1325					
50	1366					
51	1399					
52	1401					
53						
54						
55						
56						
57						
58	1579	5				
59	1624	5,18				
60	1693	5,456				
61		7				
62						

Height (mm)	Test 1 20140318 P-0.35-C50-UNS-LONG		Test 2 20140324 P-0.35-C50-UNS-LONG		Test 3 20140325 P-0.35-C50-UNS-LONG	
	Image no	time (s)	Image no	time (s)	Image no	time (s)
0	163	0	109	0	132	0
1						
2						
3						
4						
5						
6						
7						
8						
9						
10						
11	164	0,004				
12						
13						
14	238	0,3			137	0,02
15	292	0,516			138	0,024
16	334	0,684			146	0,056
17	367	0,816			768	2,544
18	377	0,856	113	0,016	938	3,224
19	389	0,904	250	0,564	1074	3,768
20	395	0,928	271	0,648	1270	4,552
21	406	0,972	330	0,884	1543	5,644
22	419	1,024	388	1,116	2222	8,36
23	447	1,136	455	1,384	2470	9,352
24	513	1,4	469	1,44	2533	9,604
25	555	1,568	494	1,54	2568	9,744
26	559	1,584	500	1,564	2617	9,94
27	564	1,604	506	1,588	2763	10,524
28	571	1,632	513	1,616	3557	13,7
29	581	1,672	524	1,66	3751	14,476
30	587	1,696	534	1,7	3969	15,348
31	591	1,712	547	1,752	4031	15,596
32	600	1,748	555	1,784	4085	15,812
33	606	1,772	564	1,82	4103	15,884
34	663	2	586	1,908	4220	16,352
35	687	2,096	611	2,008	4565	17,732
36	751	2,352	747	2,552	5223	20,364
37	797	2,536	892	3,132	7630	29,992
38	1024	3,444	1177	4,272	14492	57,44
39			2330	8,884		
40						
41						
42						

Height (mm)	Test 1 20140320 P-0.43-C50-UNS-LONG		Test 2 20140321 P-0.43-C50-UNS-LONG		Test 3 20140324 P-0.43-C50-UNS-LONG	
	Image no	time (s)	Image no	time (s)	Image no	time (s)
0	624	0	274	0	167	0
1						
2						
3						
4						
5						
6						
7						
8						
9						
10					169	0,008
11						
12			276	0,008	181	0,056
13			277	0,012	185	0,072
14			408	0,536	400	0,932
15			416	0,568	409	0,968
16	630	0,024			419	1,008
17	671	0,188	495	0,884		
18			526	1,008	467	1,2
19			579	1,22	501	1,336
20	734	0,44	627	1,412	543	1,504
21	757	0,532	661	1,548	595	1,712
22	780	0,624	730	1,824	643	1,904
23	825	0,804	802	2,112	741	2,296
24	852	0,912	832	2,232	781	2,456
25	869	0,98	856	2,328	827	2,64
26	892	1,072	905	2,524	928	3,044
27	943	1,276	963	2,756	993	3,304
28	1014	1,56	1101	3,308	1741	6,296
29	1561	3,748	2122	7,392	1954	7,148
30	1736	4,448	2304	8,12	2010	7,372
31	1841	4,868	2472	8,792	2058	7,564
32			3123	11,396	2086	7,676
33					2113	7,784
34						
35						
36						
37						
38						
39						
40						
41						
42						
43						
44						
45						

APPENDIX D

Natural Crack equilibrium rise height

	Natural Crack Width (mm)	Natural Final Height (mm)
C20 UNSAT	0,5	22,5
C20 UNSAT	1	12
C20 UNSAT	1,5	10
C20 UNSAT	1,5	5,5
C20 UNSAT	1,5	8,5
C20 UNSAT	2	6,85
C20 UNSAT	0,5	21
C20 UNSAT	1	8
C20 UNSAT	1	7
C20 UNSAT	1,5	9
C20 UNSAT	2	5
C20 UNSAT	1,5	9
C20 UNSAT	2	5,5
C20 UNSAT	1	10
C20 UNSAT	1	8
C20 UNSAT	1,5	9
C20 UNSAT	1,5	9
C20 UNSAT	2	6
C30 UNSAT	0,5	20
C30 UNSAT	1	10
C30 UNSAT	1	11
C30 UNSAT	2	6,85
C30 UNSAT	0,5	19
C30 UNSAT	1	10
C30 UNSAT	1	10
C30 UNSAT	1,5	9
C30 UNSAT	2	6
C30 UNSAT	0,5	19,5
C50 UNSAT	1	12
C50 UNSAT	1	12,5
C50 UNSAT	2	7
C50 UNSAT	2	0
C50 UNSAT	0,5	19
C50 UNSAT	0,5	18
C50 UNSAT	0,5	19,5
C50 UNSAT	0,5	18
C50 UNSAT	1	11
C50 UNSAT	1,5	8,5

APPENDIX E. Mathcad v15 Code

Flow through variable width slot $ORIGIN := 1$

Geometry

$nseg := 4$ $np := 5$ $iseg := 1 .. nseg$ $ip := 1 .. np$ **Number of segments**

$h := 0.3$ **m height of the specimen in metres**

Fluid data.

$\mu := 0.001221$ **Pa s Viscosity** $\rho := 1000$ **kg/m^3 Density** $g := 9.81$ **m/s^2 Gravitational constant**

$\theta := 22.8 \cdot deg$ **deg contact angle** $\gamma := 0.0728$ **N/m surface tension**

Set b up as varying from b_0 to bh over a height of h $r := 0.0002$ **crack width in m**

$b_0 := r$ **m Opening at base** $b_h := r$ **m Opening at top of crack**

$$b(x) := b_0 - \left(b_0 - b_h\right) \cdot \frac{x}{h} \qquad p_c(z) := 2 \cdot \frac{\gamma \cdot \cos(\theta)}{b(z)} \qquad k(x) := \frac{b(x)^2}{12}$$

$A(x) := b(x) \cdot 1$

$\phi := 90 \cdot deg$ **angle of interface**

$$\eta(z) := \mu \cdot A(z) \cdot \int_0^z \frac{1}{A(x) \cdot k(x)}\, dx$$ **Function to carryout integral 1/r from 0 to z**

$z_1 := 0.0001$ **Set initial value of z_0**

$t_1 := 0$

$\Delta t := 0.001$ **Set time step**

$nstep := 85000$ $i := 1 .. nstep$

$$t_{i+1} := t_i + \Delta t$$

$$z_{i+1} := if\left[z_i + \frac{\Delta t}{\eta(z_i)} \cdot \left(p_c(z_i) - \rho \cdot g \cdot z_i \cdot \sin(\phi)\right) < h, \left[z_i + \frac{\Delta t}{\eta(z_i)} \cdot \left(p_c(z_i) - \rho \cdot g \cdot z_i \cdot \sin(\phi)\right)\right], h\right]$$

Alternative solution

$\omega := 0.01$

$$func(z, zzn) := zzn - \left[z + \Delta t \cdot \left[\frac{r \cdot \gamma \cdot \cos(\theta)}{4 \cdot \mu \cdot [\omega \cdot zzn + (1 - \omega) \cdot z]} - \frac{r^2 \cdot \rho \cdot g}{12 \cdot \mu}\right]\right] \qquad z1 := 0.0001 \qquad zzn1 := z1$$

$$func(z1, zzn) := \left(\frac{zzn - z1}{\Delta t} + \frac{r^2 \cdot \rho \cdot g}{8 \cdot \mu}\right) \cdot [4 \cdot \mu \cdot [\omega \cdot zzn + (1 - \omega) \cdot z1]] + r \cdot \gamma \cdot \cos(\theta)$$

$zznf(z1, zzn1) := root[(func(zzn1, z1)), zzn1]$ $zznf(z1, z1) = 1.737 \times 10^{-3}$

$zzn_1 := z_1$

$zz_1 := z_1 = 1 \times 10^{-4}$

$$zzn_{i+1} := zzn_i + \Delta t \cdot \left(\frac{r \cdot \gamma \cdot \cos(\theta)}{4 \cdot \mu \cdot zzn_i} - \frac{r^2 \cdot \rho \cdot g}{8 \cdot \mu} \right)$$

Basic numerical solution

$$zzf(z) := \left| \begin{array}{l} z\theta \leftarrow z \\ \text{for } it \in 1..2 \\ \quad \left| \begin{array}{l} zzn \leftarrow z + \Delta t \cdot \left(\frac{r \cdot \gamma \cdot \cos(\theta)}{4 \cdot \mu \cdot z\theta} - \frac{r^2 \cdot \rho \cdot g}{8 \cdot \mu} \right) \\ zp \leftarrow z \\ [z\theta \leftarrow \omega \cdot zzn + (1 - \omega) \cdot zp] \end{array} \right. \\ zzn \end{array} \right.$$

$zz_{i+1} := zzf(zz_i)$

$p_c(r) = 671.116$

$p_{c1} := \frac{2 \cdot \gamma \cdot \cos(\theta)}{r} = 671.116$

Numerical solution with dynamic friction term at meniscus βm and inadditional wall friction

$$zzf1(z, \beta_s, \beta_m, \beta_w) := \left| \begin{array}{l} z\theta \leftarrow z \\ \text{for } it \in 1..2 \\ \quad \left| \begin{array}{l} zzn \leftarrow z + \frac{\Delta t \cdot \left[p_c(r) \cdot (1 - \beta_s) - \rho \cdot g \cdot z\theta \right]}{\left[\frac{2 \cdot \beta_m}{r} + \left(\frac{z}{\frac{r^2}{12 \cdot \mu} + \frac{r \cdot \beta_w}{2}} \right) \right]} \\ zp \leftarrow z \\ [z\theta \leftarrow \omega \cdot zzn + (1 - \omega) \cdot zp] \end{array} \right. \\ zzn \end{array} \right.$$

$\beta_s := 0$

$\beta_m := 0$

$\beta_w := 0$

$zz\beta s1_1 := z_1$

$zz\beta s1_{i+1} := zzf1(zz\beta s1_i, \beta_s, 0, 0)$

$zz\beta s2_1 := z_1$

$zz\beta s2_{i+1} := zzf1[zz\beta s2_i, (5 \cdot \beta_s), 0, 0]$

$zz\beta s3_1 := z_1$

$zz\beta s3_{i+1} := zzf1[zz\beta s3_i, (10 \cdot \beta_s), 0, 0]$

$zz\beta m1_1 := z_1$

$zz\beta m1_{i+1} := zzf1(zz\beta m1_i, 0, \beta_m, 0)$

$zz\beta m2_1 := z_1$

$zz\beta m2_{i+1} := zzf1[zz\beta m2_i, 0, (5 \cdot \beta_m), 0]$

$zz\beta m3_1 := z_1$

$zz\beta m3_{i+1} := zzf1[zz\beta m3_i, 0, (10 \cdot \beta_m), 0]$

$zz\beta w1_1 := z_1$

$zz\beta w1_{i+1} := zzf1(zz\beta w1_i, 0, 0, \beta_w)$

$zz\beta w2_1 := z_1$

$zz\beta w2_{i+1} := zzf1[zz\beta w2_i, 0, 0, (5 \cdot \beta_w)]$

$zz\beta w3_1 := z_1$

$zz\beta w3_{i+1} := zzf1[zz\beta w3_i, 0, 0, (10 \cdot \beta_w)]$

$a := \frac{\gamma \cdot r \cdot \cos(\theta)}{4 \cdot \mu}$

$bb := \frac{\rho \cdot g \cdot r^2}{8 \cdot \mu}$

$$W(x) := -1 + \frac{\sqrt{2 + 2 \cdot e \cdot x}}{1 + \frac{4.13501 \cdot \sqrt{2 + 2 \cdot e \cdot x}}{12.7036 + \sqrt{2 + 2 \cdot e \cdot x}}}$$

$$zpap(t) := \frac{a}{bb} \cdot \left(1 + W\left(-e^{-1 - bb^2 \cdot \frac{t}{a}} \right) \right)$$

Theoretical Rise Height

z_{theo}

$\frac{2 \cdot \gamma \cdot \cos(\theta)}{r \cdot \rho \cdot g} \cdot 1000 = 68.411$